DE82006094

NTIS
One Source. One Search. One Solution.

CHEMISTRY AND CATALYSIS OF COAL LIQUEFACTION CATALYTIC AND THERMAL UPGRADNG OF COAL LIQUID AND HYDROGENATION OF CO TO PRODUCE FUELS. QUARTERLY PROGRESS REPORT, JULY-SEPTEMBER 1981

UTAH UNIV., SALT LAKE CITY. DEPT. OF MINING AND FUELS ENGINEERING

DEC 1981

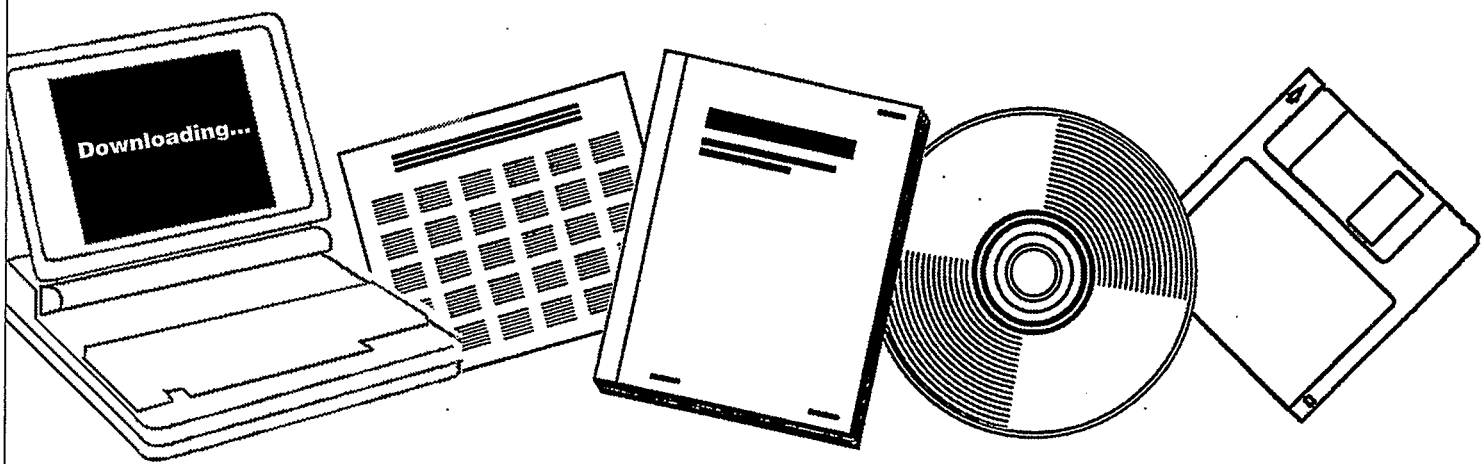

U.S. Department of Commerce
National Technical Information Service

DOE/ET/14700-8
(DE82006094)
Distribution Category UC-90d

DE82006094

Chemistry and Catalysis of Coal Liquefaction Catalytic and Thermal Upgrading of Coal Liquid and Hydrogenation of CO to Produce Fuels

Quarterly Progress Report
for the Period July-Sept 1981

Dr. Wendell H. Wiser

University of Utah - Department of
Mining and Fuels Engineering
Salt Lake City, Utah 84112

Date Published - December 1981

Prepared for the United States Department
of Energy
Under Contract No. DE-AC22-79Et14700

CONTENTS

OBJECTIVE AND SCOPE OF WORK

I. The chemistry and Catalysis of Coal Liquefaction

Task 1 Chemical-Catalytic Studies

Coal will be reacted at subsoftening temperatures with selective reagents to break bridging linkages between clusters with minimal effect on residual organic clusters. The coal will be pretreated to increase surface area and then reacted at 25 to 350°C. Reagents and catalysts will be used which are selective so that the coal clusters are solubilized with as little further reaction as possible.

Task 2 Carbon-13 NMR Investigation of CDL and Coal

Carbon-13 NMR spectroscopy will be used to examine coal, coal derived liquids (CDL) and residues which have undergone subsoftening reactions in Task 1 and extraction. Improvements in NMR techniques, such as crosspolarization and magic angle spinning, will be applied. Model compounds will be included which are representative of structural units thought to be present in coal. Comparisons of spectra from native coals, CDL and residues will provide evidence for bondings which are broken by mild conditions.

Task 3 Catalysis and Mechanism of Coal Liquefaction

This fundamental study will gain an understanding of metal salt chemistry and catalysis in coal liquefaction through study of reactions known in organic chemistry. Zinc chloride and other catalytic materials will be tested as Friedel-Crafts catalysts and as redox catalysts using coals and selected model compounds. Zinc chloride, a weak Friedel-Crafts catalyst, will be used at conditions common to coal liquefaction to participate in well defined hydrogen transfer reactions. These experiments will be augmented by mechanistic studies of coal hydrogenation using high pressure thermogravimetric analysis and structural analysis. The results of these studies will be used to develop concepts of catalysis involved in coal liquefaction.

Task 4 Momentum Heat and Mass Transfer in CoCurrent Flow of Particle-Gas Systems for Coal Hydrogenation

A continuation of ongoing studies of heat and transport phenomena in cocurrent, co-gravity flow is planned for a one-year period. As time and development of existing work permits, the extension of this study to include a coiled reactor model will be undertaken. Mathematical models of coal hydrogenation systems will utilize correlations from these straight and coiled reactor configurations.

Task 5 The Fundamental Chemistry and Mechanism of Pyrolysis of Bituminous Coal

Previous work at the University of Utah indicates that coal pyrolysis, dissolution (in H-donor) and catalytic hydrogenation all have similar rates and activation energies. A few model compounds will be pyrolyzed in the range of 375 to 475°C. Activation energies, entropies and pro-

duct distributions will be determined. The reactions will assist in formulating the thermal reaction routes which also can occur during hydro-liquefaction.

II. Catalytic and Thermal Upgrading of Coal Liquids

Task 6 Catalytic Hydrogenation of CD Liquids and Related Polycyclic Aromatic Hydrocarbons

A variety of coal derived (CD) liquids will be hydrogenated with sulfided catalysts prepared in Task 10 from large pore, commercially available supports. The hydrogenation of these liquids will be systematically investigated as a function of catalyst structure and operating conditions. The effect of extent of hydrogenation will be the subject of study in subsequent tasks in which crackability and hydropyrolysis of the hydrogenated product will be determined. To provide an understanding of the chemistry involved, model polycyclic arenes will be utilized in hydrogenation studies. These studies and related model studies in Task 7 will be utilized to elucidate relationships between organic reactants and the structural-topographic characteristics of hydrogenation catalysts used in this work.

Task 7 Denitrogenation and Deoxygenation of CD Liquids and Related Nitrogen- and Oxygen-Containing Compounds

Removal of nitrogen and oxygen heteroatoms from CD liquids is an important upgrading step which must be accomplished to obtain fuels corresponding to those from petroleum sources. Using CD liquids as described in Task 6, exhaustive HDN and HDO will be sought through study of catalyst systems and operating conditions. As in Task 6, catalysts will be prepared in Task 10 and specificity for N- and O-removal will be optimized for the catalyst systems investigated. Model compounds will also be systematically hydrogenated using effective HDN/HDO catalysts. Kinetics and reaction pathways will be determined. A nonreductive denitrogenation system will be investigated using materials which undergo reversible nitridation. Conditions will be sought to cause minimal hydrogen consumption and little reaction of other reducible groups.

Task 8 Catalytic Cracking of Hydrogenated CD Liquids and Related Polycyclic Naphthenes and Naphthenoaromatics

Catalytic cracking of hydrogenated CD liquid feedstocks will be studied to evaluate this scheme as a means of upgrading CD liquids. Cracking kinetics and product distribution as a function of preceding hydrogenation will be evaluated to define upgrading combinations which require the minimal level of CD liquid aromatic saturation to achieve substantial heteroatom removal and high yields of cracked liquid products. Cracking catalysts to be considered for use in this task shall include conventional zeolite-containing catalysts and large-pore molecular sieve, CLS (cross-linked smectites) types under study at the University of Utah. Model compounds will be subjected to tests to develop a mechanistic understanding of the reactions of hydro CD liquids under catalytic cracking conditions.

Task 9 Hydropyrolysis (Thermal Hydrocracking) of CD Liquids

Heavy petroleum fractions can be thermally hydrocracked over a specific range of conditions to produce light liquid products without excessive hydrogenation occurring. This noncatalytic method will be applied to a variety of CD liquids and model compounds, as mentioned in Task 6, to determine the conditions necessary and the reactibility of these CD feedstocks with and without prior hydrogenation and to derive mechanism and reaction pathway information needed to gain an understanding of the hydropyrolysis reactions. Kinetics, coking tendencies and product compositions will be studied as a function of operating conditions.

Task 10 Systematic Structural-Activity Study of Supported Sulfide Catalysts for Coal Liquids Upgrading

This task will undertake catalyst preparation, characterization and measurement of activity and selectivity. The work proposed is a fundamental study of the relationship between the surface-structural properties of supported sulfide catalysts and their catalytic activities for various reactions desired. Catalysts will be prepared from commercially available. Supports composed of alumina, silica-alumina, silica-magnesia and silica-titania, modification of these supports to change acidity and to promote interaction with active catalytic components is planned. The active constituents will be selected from those which are effective in a sulfided state, including but not restricted to Mo, W, Ni and Co. The catalysts will be presulfided before testing. Catalyst characterization will consist of physico-chemical property measurements and surface property measurements. Activity and selectivity tests will also be conducted using model compounds singly and in combination.

Task 11 Basic Study of the Effects of Coke and Poisons on the Activity of Upgrading Catalysts

This task will begin in the second year of the contract after suitable catalysts have been identified from Tasks 6, 7 and/or 10. Two commercial catalysts or one commercial catalyst and one catalyst prepared in Task 10 will be selected for a two-part study, (1) simulated laboratory poisoning/coking and (2) testing of realistically aged catalysts. Kinetics of hydrogenation, hydrodesulfurization, hydrodenitrogenation and hydrocracking will be determined before and after one or more stages of simulated coking. Selected model compounds will be used to measure detailed kinetics of the above reactions and to determine quantitatively how kinetic parameters change with the extent and type of poisoning/coking simulated. Realistically aged catalysts will be obtained from coal liquids upgrading experiments from other tasks in this program or from other laboratories conducting long-term upgrading studies. Deactivation will be assessed based on specific kinetics determined and selective poisoning studies will be made to determine characteristics of active sites remaining.

Task 12 Diffusion of Polyaromatic Compounds in Amorphous Catalyst Supports

If diffusion of a reactant species to the active sites of the catalyst is slow in comparison to the intrinsic rate of the surface reaction, then only sites near the exterior of the catalyst particles will be utilized effectively. A systematic study of the effect of molecular size on the sorptive diffusion kinetics relative to pore geometry will

be made using specific, large diameter aromatic molecules. Diffusion studies with narrow boiling range fractions of representative coal liquid will also be included. Experimental parameters for diffusion kinetic runs shall include aromatic diffusion model compounds, solvent effects, catalyst sorption properties, temperature and pressure.

III. Hydrogenation of CO to Produce Fuels

Task 13 Catalyst Research and Development

Studies with iron catalysts will concentrate on promoters, the use of supports and the effects of carbiding and nitriding. Promising promoters fall into two classes: (1) nonreducible metal oxides, such as CaO, K_2O, Al_2O_3 and MgO, and (2) partially reducible metal oxides which can be classified as co-catalysts, such as oxides of Mn, Mo, Ce, La, V, Re and rare earths. Possible catalyst supports include zeolites, alumina, silica, magnesia and high area carbons. Methods of producing active supported iron catalysts for CO hydrogenation will be investigated, such as development of shape selective catalysts which can provide control of product distribution. In view of the importance of temperature, alternative reactor systems (to fixed bed) will be investigated to attain better temperature control. Conditions will be used which give predominately lower molecular weight liquids and gaseous products.

Task 14 Characterization of Catalysts and Mechanistic Studies

Catalysts which show large differences in selectivity in Task 13 will be characterized as to surface and bulk properties. Differences in properties may provide the key to understanding why one catalyst is superior to another and identify critical properties, essential in selective catalysts. Factors relating to the surface mechanism of CO hydrogenation will also be investigated. Experiments are proposed to determine which catalysts form "surface" (reactive) carbon and the ability of these catalysts to exchange C and O of isotopically labelled CO. Reactions of CO and H_2 at temperatures below that required for CO dissociation are of particular interest.

Task 15 Completion of Previously Funded Studies and Exploratory Investigations

This task is included to provide for the orderly completion of coal liquefaction research underway in the expiring University of Utah contract, EX-76-C-01-2006.

III Highlights to Date

The hydrogenation activity of a series of HDS catalysts correlated well with O_2 chemisorption and surface dispersion measured by ESCA; however, the HDS activity showed poor correlation with both techniques. The implication is that hydrogenation most likely takes place at edge sites on the basic MoS_2 crystallites and HDS at different, yet unknown site locations.

Chemisorption, X-ray diffraction and ESCA measurements have demonstrated that MnO is concentrated on the surface of the basic Fe particles in reduced Fe-Mn Fischer Trposch catalysts.

Papers and Presentations

"Chemical Structure of Heavy Oils Derived from Coal Hydrogenation Determined by Mass Spectroscopy," S. Yokoyama, N. Tsuzuki, T. Katoh, Y. Sanada, D.M. Bodily and W.H. Wiser, Coal Structure, M.L. Gorbaty and K. Ouchi, Ed., Advances in Chemistry Series 192, American Chemical Society, Washington, D.C., 1981, p. 257.

"Microscopic Examination of Residues from Short Residence-Time Catalytic Hydrogenation of Bituminous Coal," D.M. Bodily, M. Shibaoka and R. Yoshida, Preprints, International Conference on Coal Science, Dusseldorf, Germany, September 7-9, 1981, p. 350.

Task 1

Chemical-Catalytic Studies of Coal Liquefaction

Faculty Advisor: J. Shabtai
Graduate Student: R. Jensen

Introduction

This project is concerned with the development of suitable processing conditions and catalyst-solvent systems for coal liquefaction under mild temperature (<350°C) and pressure (<2000 psi).

Project Status

One of the main conditions for effective use of catalyst-solvent systems in liquefaction below the coal softening point is the necessity of increasing the micorpore volume of the solide coal. Previous studies in this department show that pretreatment of coal with metal halides, e.g., $ZnCl_2$, at relatively mild temperatures (200-350°C) causes considerable increase in surface area and microporosity. Elucidation of the nature of chemical reactions between metal halides and coal has attracted recently considerable interest. In the framework of our work on homogeneously catalyzed liquefaction, it was considered of importance to develop a better understanding of such reactions. Therefore, systematic studies of metal halide-catalyzed reactions were undertaken, using the following types of model compounds:

(a) Alkylbenzenes with branched alkyl groups;

(b) Alkylbenzenes with n-alkyl groups; and

(c) Diarylalkanes.

These studies were intended to provide information on (1) the mode of catalytic activity of metal halides in a wide range of experimental conditions; and (2) the direction and rate of metal halide-catalyzed dealkyation and hydrodealkylation processes, as related to cleavage reactions of intercluster linkages in the coal structure.

The previous reports (DE/ET/14700-6 and 14700-7) described the results obtained in a systematic study of hydrodealkylation reactions of representative monoalkylbenzenes of type (a), i.e., isopropylbenzene (2), sec-butylbenzene (3) and tert-butylbenzene (1), in the presence of a supported $ZnCl_2$ catalyst. Subsequently, the dealkylation reactions of representative monoalkylbenzenes having normal alkylsubstituents, i.e., n-propylbenzene, n-butylbenzene, and n-hexylbenzene, in the presence of the same type of silica gel-supported $ZnCl_2$ catalyst (see preceding report), were systematically investigated in the 250-400°C temperature range. Experiments were carried out under a hydrogen pressure of 850 psig, using the same micro-reactor employed previously. The total reaction time in each run was kept constant at 90 seconds. Products obtained were identified and quantitatively analyzed by a combination of gas chromatography and mass spectrometry.

Table 1 summarizes the change in product composition from the $ZnCl_2$-catalyzed hydrodealkylation of n-propylbenzene (4) as a function of reaction temperature (250-400°C). As seen, the conversion of 4 is generally very low but increases somewhat with increase in temperature (from 0.3 to 3.3%). It is also observed that the conversion of 4 is sharply lower than that of the isomeric cumene (1.2 to 20.9% by wt at 250-400°C, Table 2). The selectivity of hydrodealkylation of 4 to yield benzene is appreciable only at 400°C (ca. 60% by wt). At 300°C there are competitive side-chain dealkylation reactions to yield toluene and ethylbenzene as major products (total yield, 68% by wt). The above changes in liquid product composition as a function of temperature are correlated with corresponding changes in gas product composition. At low temperature (250°C) the main products are methane (54%) and ethane plus ethylene (total yield, 34.2%), but as temperature is increased the concentration of these products decreases while the concentration of C_3 gases, viz., propane and propene, increases (yield, 67% at 400°C).

Table 2 provides data on the product composition from $ZnCl_2$- catalyzed hydrodealkylation of n-butylbenzene (5) at a reaction temperature of 350°C, using a reaction time of 90 seconds and a hydrogen pressure of 850 psig. As seen, the conversion of 5 under these conditions is very low, viz., 4.7% by wt. This conversion is drastically lower, as compared to that of the isometric t-butylbenzene (1) under the same set of conditions (41.1%). The results obtained with compounds 4 and 5 clearly indicate that n-alkylbenzenes are much less susceptible to $ZnCl_2$-catalyzed hydrodealkylation, as compared to alkylbenzenes with branched alkyl groups (see mechanistic discussion). The selectivity of the simple hydrodealkylation reaction of 5, to yield benzene, is moderate (55.3%). Competitive side-chain dealkylation reactions, yielding toluene and ethylbenzene (plus styrene), also occur to a significant extent (total yield, 37%). The gaseous product from hydroalkylation of compound 5 contains in addition to the anticipated C_4 hydrocarbons (yield, 18.3%) large amounts of C_2 and C_3 hydrocarbons (yield, 47.5% and 24.9%, respectively). The C_1-C_3 gaseous products are probably derived to a large extent by secondary decomposition reactions of the butyl carbonium ion formed in the initial dealkylation step of the reaction (see mechanistic discussion).

Table 3 provides data on the product composition from the $ZnCl_2$-catalyzed hydrodealkylation of n-hexylbenzene (6) at 350°C, using a reaction time of 90 seconds and a hydrogen pressure of 850 psig. As seen, the conversion of 6 under these conditions is ca. 12.3%, indicating somewhat higher reactivity of this compound as compared to compounds 4 and 5. The main liquid product is t-butylbenzene (ca. 58.0%) which is apparently derived by secondary realkylation reaction of the primary dealkylation product, benzene (see mechanistic discussion). Other important liquid products found include ethylbenzene and styrene. The gaseous product consists mostly of C_2-C_4 hydrocarbons, which are probably derived to a large extent by secondary splitting reactions of the hexyl carbonium ion formed in the initial dealkylation step (see below).

The indicated very low rate of $ZnCl_2$-catalyzed hydrodealkylation of n-alkylbenzenes, e.g., compounds 4, 5 and 6 at 250-400°C can be attributed to the necessity of a thermodynamically unfavorable intermediate step in such a reaction, leading to an unstable primary carbonium ion:

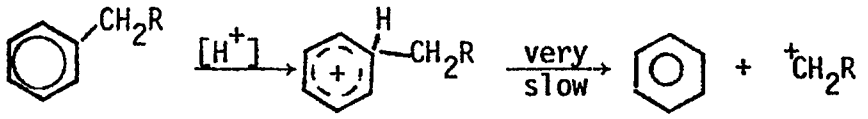

The results obtained indicate that protonic acid-catalyzed reactions of this type are not only very slow, but also not very selective due to the occurrence (also at very low rate) of competing reactions viz., (a) Lewis acid-catalyzed side-chain dealkylation; and (b) thermal cracking of the β-bond in the n-alkyl substituent. In addition, the unstable primary carbonium ion produced by proton-catalyzed dealkylation of the n-alkylbenzene undergoes fast rearrangement and/or cleavage reactions leading to an important extent to gaseous products with lower carbon number than the carbon number of the n-alkyl group in the feed. As a result the composition of gaseous products from dealkylation reactions of n-alkylbenzenes is much more complex than that observed with alkylbenzenes having tertiary or secondary alkyl substituents. The product compositions from compounds 4, 5 and 6 can be rationalized in terms of the following probable mechanistic schemes.

(a) n-Propylbenzene (4)

At sufficiently high temperature, e.g., 400°C, the main reaction is proton-catalyzed hydrodealkylation:

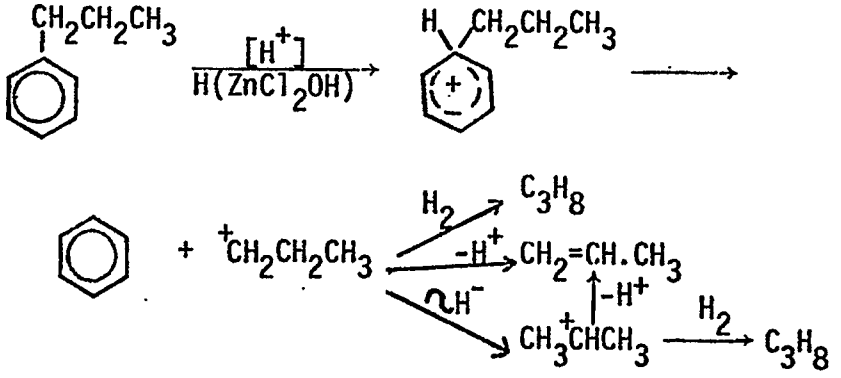

At lower temperatures (250-300°C) this reaction is accompanied by Lewis acid-catalyzed side-chain dealkylation:

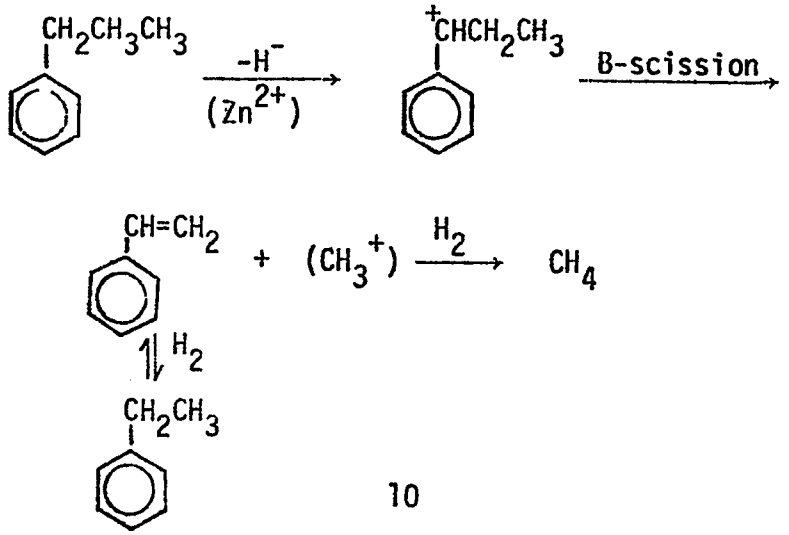

The formation of some toluene may be due to a very limited extent of thermal cracking of 4:

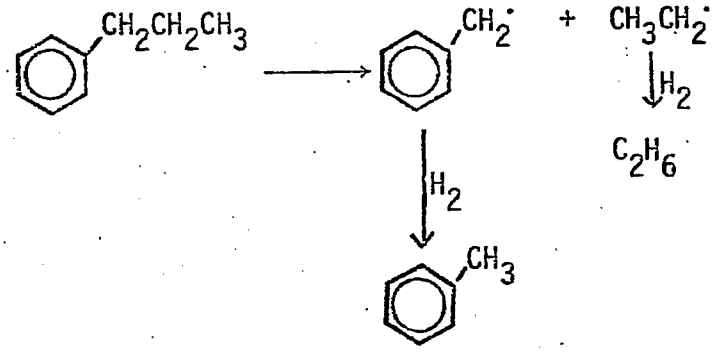

(b) n-Butylbenzene (5)

As in the case of compound 4, the main reaction observed at 350°C is proton-catalyzed dealkylation. The primary n-butyl carbonium ion undergoes considerable secondary cleavage and rearrangement reactions:

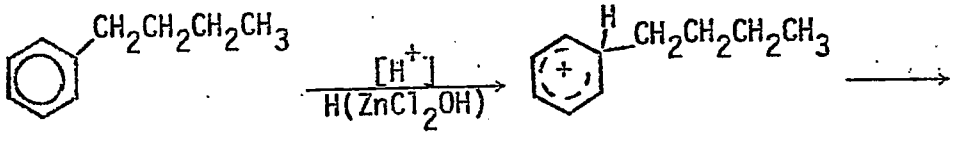

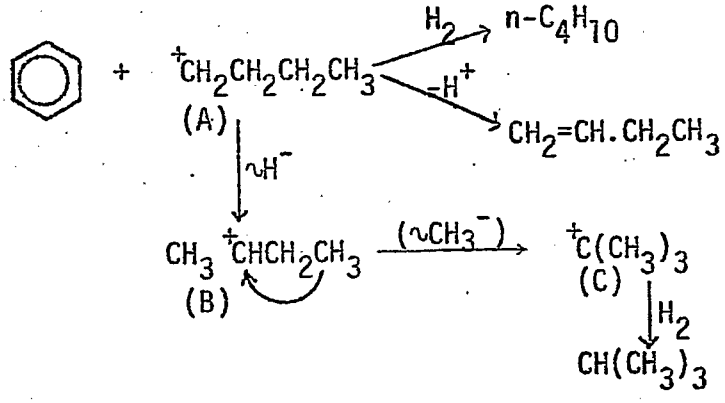

The t-butyl carbonium ion (C), derivde by stepwise rearrangement of the initial primary carbonium ion (A), apparently realkylates some of the benzene produced to form t-butylbenzene (Table 2, footnote d).

The carbonium ions (A) and (B) are also subjected to β-scission reactions leading to C_1-C_3 gaseous products (Table 8):

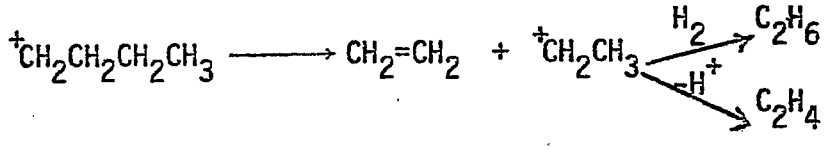

(c) n-Hexylbenzene (6)

The $ZnCl_2$-catalyzed conversion of compound 6 at 350°C (Table 3) is somewhat higher than that of n-butylbenzene (5) at the same temperature, indicating that the overall reactivity of n-alkylbenzenes for hydrodealkylation may increase to some extent with increase in the length of the n-alkyl group. The formation of t-butylbenzene as the main liquid product and the observed parallel formation of isobutane as a major gaseous product (Table 3) are apparently correlated. A plausible mechanistic scheme which could explain the formation of these compounds involves protonic acid-catalyzed hydrodealkylation of 6 to yield benzene plus n-hexyl carbonium ion (A), followed by β-scission of (A) to yield a C_2 product plus t-butyl carbonium ion (C) and, finally, realkylation of the benzene with (C):

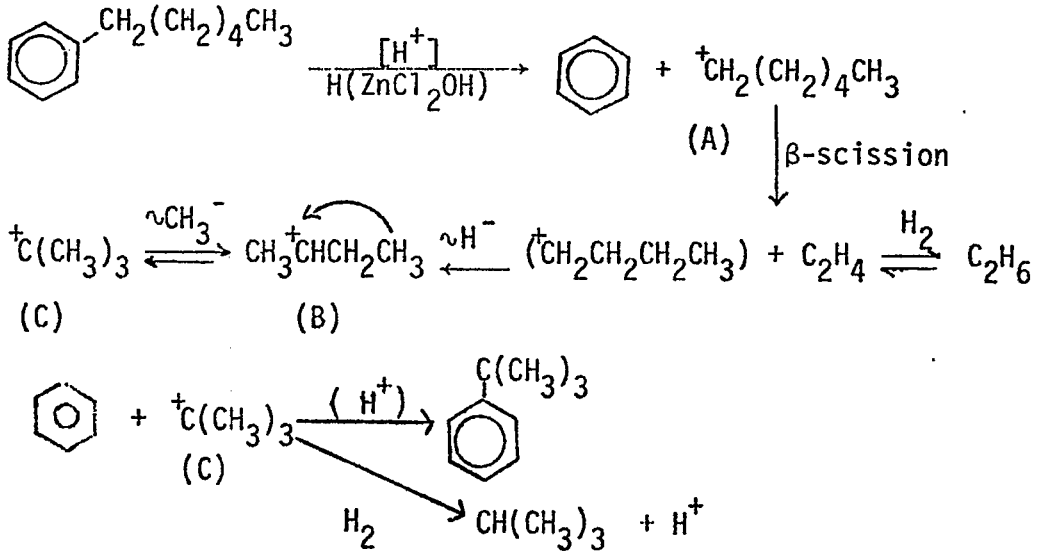

The β-cleavage of (A) may proceed by a concerted mechanism to give directly the sec-butyl carbonium ion (B):

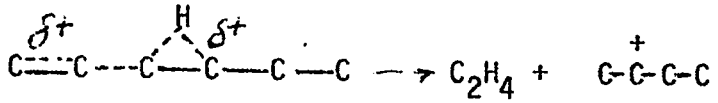

Some realkylation of the benzene with (B) apparently also takes place as evidenced by the formation of some sec-butylbenzene.

Competing Lewis acid-catalyzed reaction of the starting compound 6 could serve as an additional source of t-butyl carbonium ions (C) and isobutane:

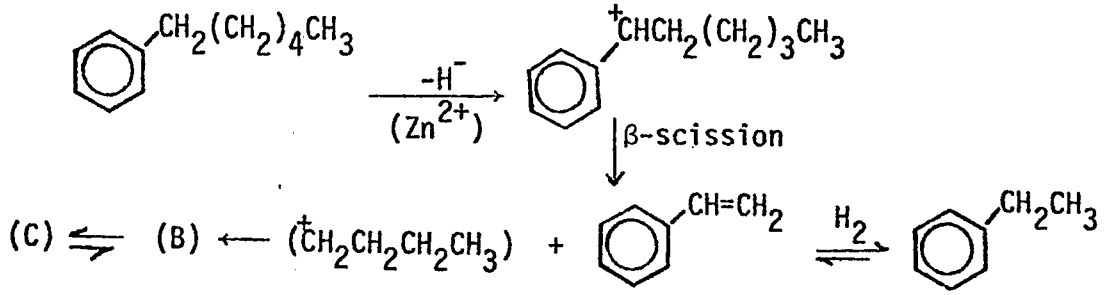

The above reaction also explains the formation of styrene and ethylbenzene as liquid products of some importance (Table 3).

It should be noted that n-alkyl-substituted arenes having long alkyl chains are found as important components of liquid products obtained by $ZnCl_2$-catalyzed coal liquefaction, both under moderate (250-350°C) and high (480-500°C) temperature conditions.[7] The results presented in this Chapter provide a plausible explanation for this observation by clearly indicating that such compounds are inherently resistant to protonic acid catalyzed hydrodealkylation. The very low rate of Friedel-Crafts dealkylation of n-alkylbenzenes indicated in this study is consistent with the anticipated high activation energy for a reaction involving the formation of a thermodynamically unfavorable primary carbonium ion.

TABLE 1

Change in Product Composition from Hydrodealkylation of n-Propylbenzene (4) as a Function of Reaction Temperature

Experiment No.	186	183	184
Reaction temperature, °C	250	300	400
Conversion of 4, mole %	0.3	1.0	3.3
Catalyst	$ZnCl_2$	$ZnCl_2$	$ZnCl_2$
Catalyst wt. %	7.1	6.5	6.4
Gaseous Product Component, mole %[c]			
CH_4	54.4	34.8	13.9
C_2H_6	26.8	12.1	2.1
C_2H_4	7.4	6.6	4.1
C_3H_8	2.0	16.58	55.0
C_3H_6	3.4	14.8	12.0
i-C_4H_{10}	4.4	10.8	8.9
n-C_4H_{10}	2.0	1.2	0.9
1-Butene	----	0.8	0.1
Isobutene	----	2.87	2.6
Liquid Product Component, mole %[c]			
Benzene	12.9	32.0	60.3
Toluene	43.5	21.7	8.9
Ethylbenzene & Styrene	43.6	46.3	21.7
Cumene	----	----	9.9

[a]In each run were used 0.15g (.001 mole) of 4 and 0.05g of 5% $ZnCl_2/SiO_2$ catalyst. [b]Hydrogen pressure, 850 psig. [c]Moles per 100 moles of reacted 4.

TABLE 2

Product Composition from Hydrodealkylation of n-Butylbenzene (5)

Experiment No.	182
Reaction Temperature, °C	350
Conversion of 5, mole %	4.7
Catalyst	$ZnCl_2$
Catalyst wt. %	6.5
Gaseous Product Component, mole %[c]	
CH_4	9.3
C_2H_6	43.2
C_2H_4	4.3
C_3H_8	20.8
C_3H_6	4.1
i-C_4H_{10}	13.3
n-C_4H_{10}	1.8
i-Butene	2.5
1-Butene	0.7
Liquid Product Component, mole %[c]	
Benzene	55.3
Toluene	9.0
Ethylbenzene & Styrene	28.0
Other components[d]	4.3

[a]In each run were used 0.15g (.001 mole) of 5 and 0.05g of 5% $ZnCl_2/SiO_2$ catalyst. [b]Hydrogen pressure, 850 psig. [c]Moles per 100 moles of reacted 5. [d]Mostly t-butylbenzene.

TABLE 3

Change in Product Composition from Hydrodealkylation of n-Hexylbenzene (6) at 350°C

Experiment No.	189
Reaction temperature, °C	350
Conversion of 6, mole %	12.3
Catalyst	$ZnCl_2$
Catalyst wt. %	7.3
Gaseous Product Component, mole %[c]	
CH_4	4.1
C_2H_6	34.7
C_2H_4	2.1
C_3H_8	13.4
C_3H_6	9.6
i-C_4H_{10}	30.2
n-C_4H_{10}	3.8
Isobutene	1.7
Liquid Product Component, mole %[c]	
Benzene	8.7
Toluene	5.1
Ethylbenzene & Styrene	18.9
n-Propylbenzene & Cumene	3.3
sec-Butylbenzene & n-butylbenzene	5.9
t-Butylbenzene	58.0

[a]In each run were used 0.15g (.001 mole) of 6 and 0.05g of 5% $ZnCl_2$ catalyst. [b]Hydrogen pressure, 850 psig. [c]Moles per 100 moles of reacted 6.

Task 3

Catalysis and Mechanism of Coal Liquefaction

Faculty Advisor: D.M. Bodily
Graduate Student: Jason Miller

Introduction

The hydroliquefaction of coal may be characterized by a mechanism which involves the initial rupture of covalent bonds to form reactive intermediates. These intermediates may be stabilized by hydrogen transfer to form lower molecular weight products or they may polymerize to form insoluble char or coke. Metal halides such as zinc chloride have been shown to be active in the bond scission stage of the reaction where as many catalysts are active only in stabilizing the intermediates, often by regenerating a hydrogen donor. The combination of thermal and catalytic reactions occurring simultaneously results in a complicated reaction mechanism. The chemistry of $ZnCl_2$ will be studied with model compounds and coal by such reactions as hydrogen transfers, cleavage of specific bonds and interaction with π electron systems.

A high performance liquid chromatograph, HPLC, will be used to analyze liquid products of the reactions under study. Further characterization of the products will be by nuclear magnetic resonance, NMR, structural analysis and vapor pressure osmometry.

Project Status

Previous work has shown that the chromatographic separations developed by Raphaelian[1] and Dark[2] could be adapted to this HPLC work on coal-derived liquids (CDL) with just minor revisions. During this quarter, work has been done to optimize these separations for CDL samples. The objective is to provide both rapid, reproducible separations and distinct fractions in sufficient quantity to allow further analysis by spectroscopic and chromatographic techniques.

Several runs showed that the optimum conditions for this objective could be made from minor revisions of the original conditions listed in the preceding quarterly report. The separation of polar, nonpolar and most polar fractions of a hexane soluble Utah CDL on the NH_2 μ Bondapak column are shown in Figure 1. This chromatogram shows the gradient used to separate the liquid sample into three distinct fractions is rather severe. Also detailed is the rate of column loading needed to collect a reasonable amount of material. The analytical column's capacity and the detectors are being driven to their limits. The very sharp, definite lines in the ΔRI trace indicate where the fraction collector switched to collect a new fraction. There is approximately 1 minute delay from the peak indication on the chromatogram to the actual collection of that peak in the collector. In this chromatrogram, the CDL is in three distinct fractions which can be collected for further analysis.

In Figure 2, the separation has also been optimized to separate the three fractions. The first major peaks are considered more polar because the retention time of the less polar and nonpolar compounds is longer due to the phenyl group functionality of the column packing. With the less severe gradient, the less polar compounds tend to elute in fraction 2 and the nonpolars and least polars tend to elute last. This has been substantiated by IR data collected on the fractions of many successive runs both with the phenyl μ Bondapak and the NH_2 μ Bondapak columns.

After these fractions from the columns were collected and evaporated down, they were subjected to IR and GC-MS analysis. Runs on the GC-MS indicated many different compounds eluting at approximately the same time, which suggested the need for several new approaches. First more extensive GC work needed to be done to generate a better separation. When optimized, using retention time standards, families of compounds could be identified and therefore a better idea of what really was appearing in the GC-MS data could be obtained. Secondly, IR work could define more clearly the major function groups present and to maybe pinpoint the differences in the fractions. Lastly, the resulting GC-MS data would have to be subjected to a very detailed analysis, looking for more specific ions resulting from some of these pinpointed functional groups.

The IR spectral work has been completed. Figures 3 and 4 are representative spectra of the intermediate polar fractions collected. These spectra pinpoint the problem. From fraction to fraction and different columns, only minor differences appear. The first major peak is -OH functional absorption @ 3300-3400 cm^{-1}. This peak varies the most from polar to nonpolar fractions. Next, is C-H absorption @ 2800-3100 cm^{-1}. Again, very little difference. Interesting to note is the strength of the ether and ester absorptions around 1720 cm^{-1} and 1275 cm^{-1}. These absorptions and minor changes in methyl and methylene absorption strength in the 1370 cm^{-1} and 1450 cm^{-1} point to possibly one ring aromatics with alot of substitutions. The absorptions from 900 cm^{-1} to 650 cm^{-1} indicate this possibility. In this range, the greatest difference exists between spectra. These are the last three peaks in the IR spectra of Figures 3 and 4. Figure 4 indicates possibly more alkyl type substitutions on the aromatic ring than exhibited in Figure 3. Again no major differences exist in the IR spectra, from all runs, except for the -OH absorptions around 3380 cm^{-1}.

Future Work

The collected fractions will be subjected to more extensive GC work to optimize separations. These conditions will be used in retention time studies. The GC-MS work will then be used to further the understanding of the compounds separated.

Finally the HPLC separations developed will be applied to various other CDL's and the fractions subjected to further HPLC, IR, GC and GC-MS analyses.

References

1. L.A. Raphaelian, Development of an HPLC, GC/MS Method for Analysis of Hygas Oil Samples, Argonne National Laboratory, ANL/EMR-4, June 1979.

2. W.A. Dark and W.H. McFadden, J. Chromatographic Science, 16, 289, July 1978.

Figure 1. Hiawatha CDL, hexane soluble
Column: NH_2-μ Bondapak
Injection Volume: 165 μl
Mobile Phase: n C_7 to 90% CH_2Cl_2/10% ETOH
Gradient: #11, 0 to 100%, 45 min

Flow Rate: 2.0 ml/min
Backflush: 15 min
Reverse to Forward: 45 min
Detectors: Bottom: UV, 254 nm, 2AUFS
Top: ΔRI, 8x

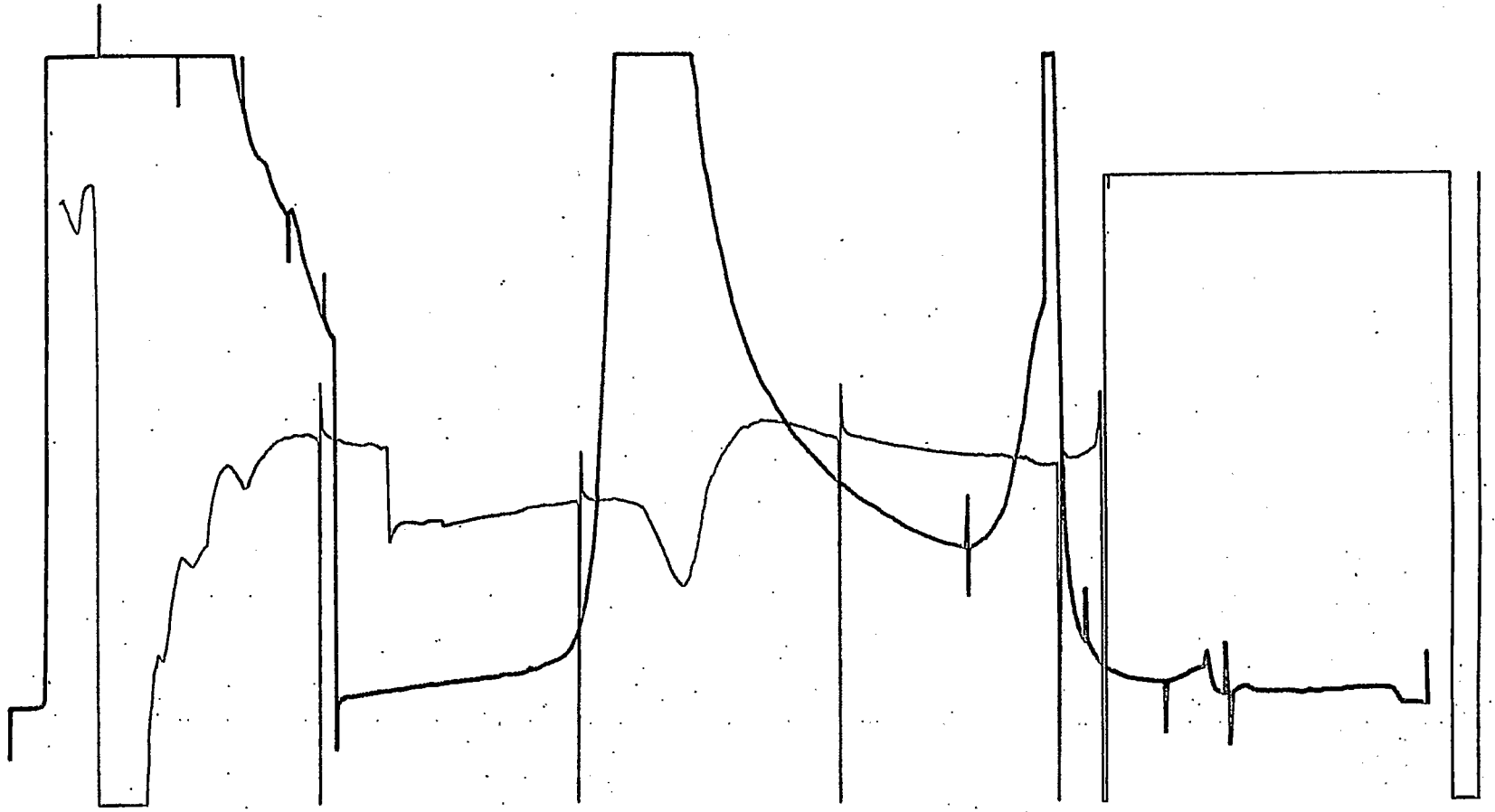

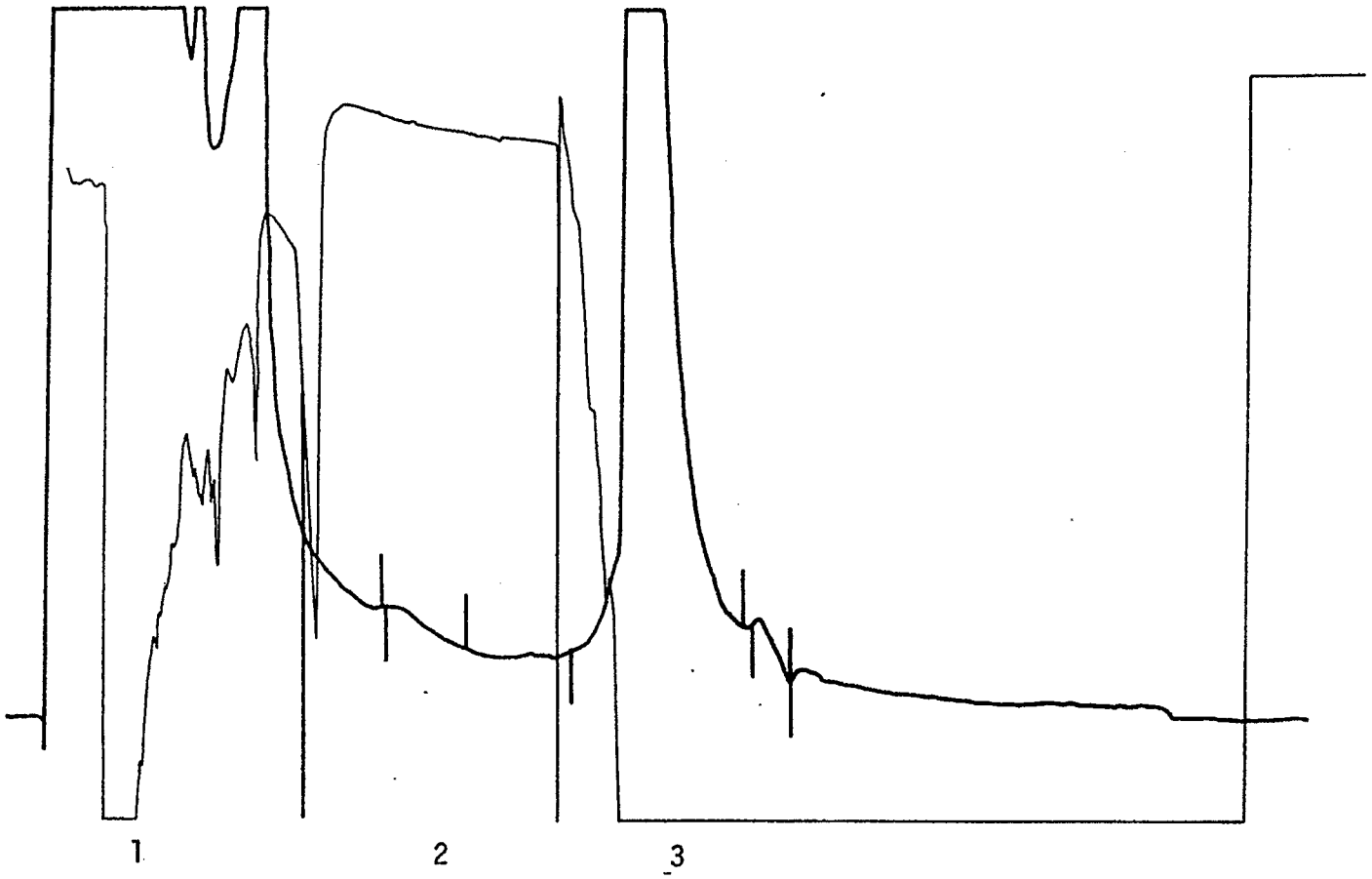

Figure 2. Hiawatha CDL, hexane soluble
Column: Phenyl μ-Bondapak
Injection Volume: 165 μl
Mobile Phase: n C_7 to 90% CH_2Cl_2/10% ETOH
Gradient: #9, 0 to 50% CH_2Cl_2 mix, 36 min.
Flow Rate: 2.0 ml/min
Detectors: Bottom: UV, 254 nm, 2AUFS
Top: ΔRI, 8x

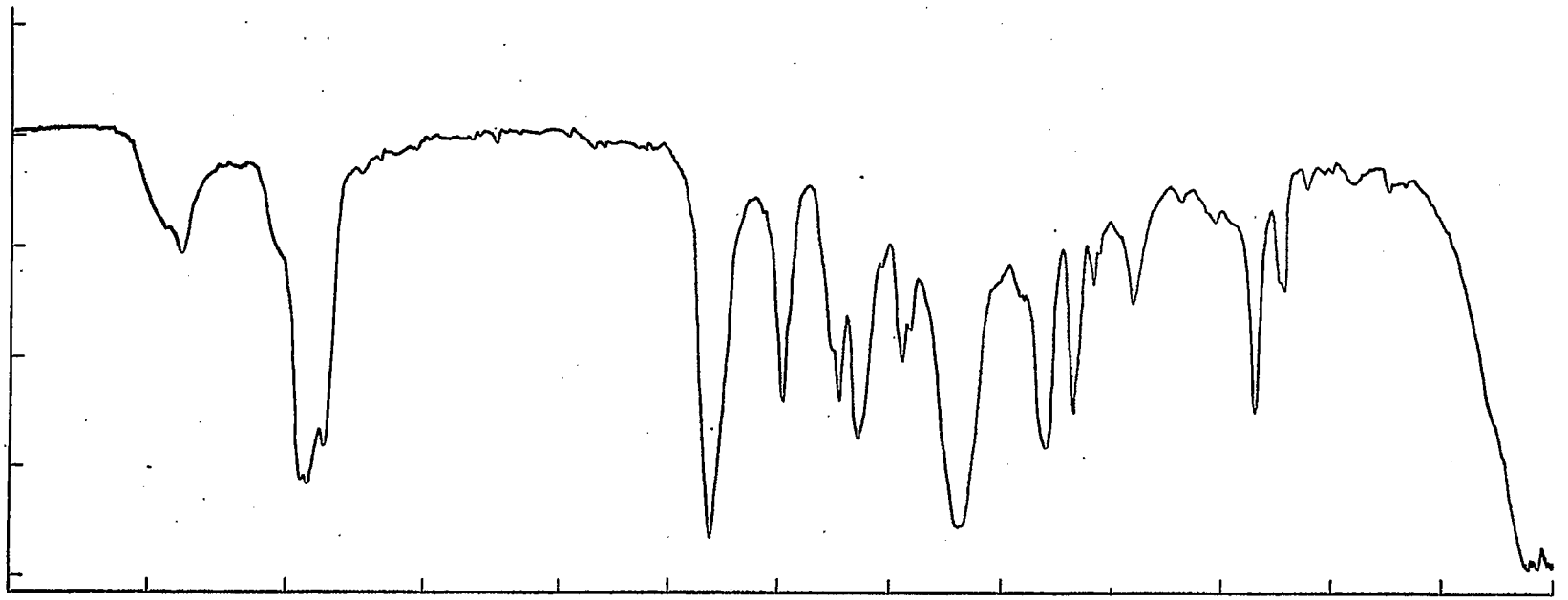

Figure 3. Hiawatha CDL, Fraction #4, from NH_2 μ-Bondapak column.
IR: 283 Perkin-Elmer in % Transmission mode.

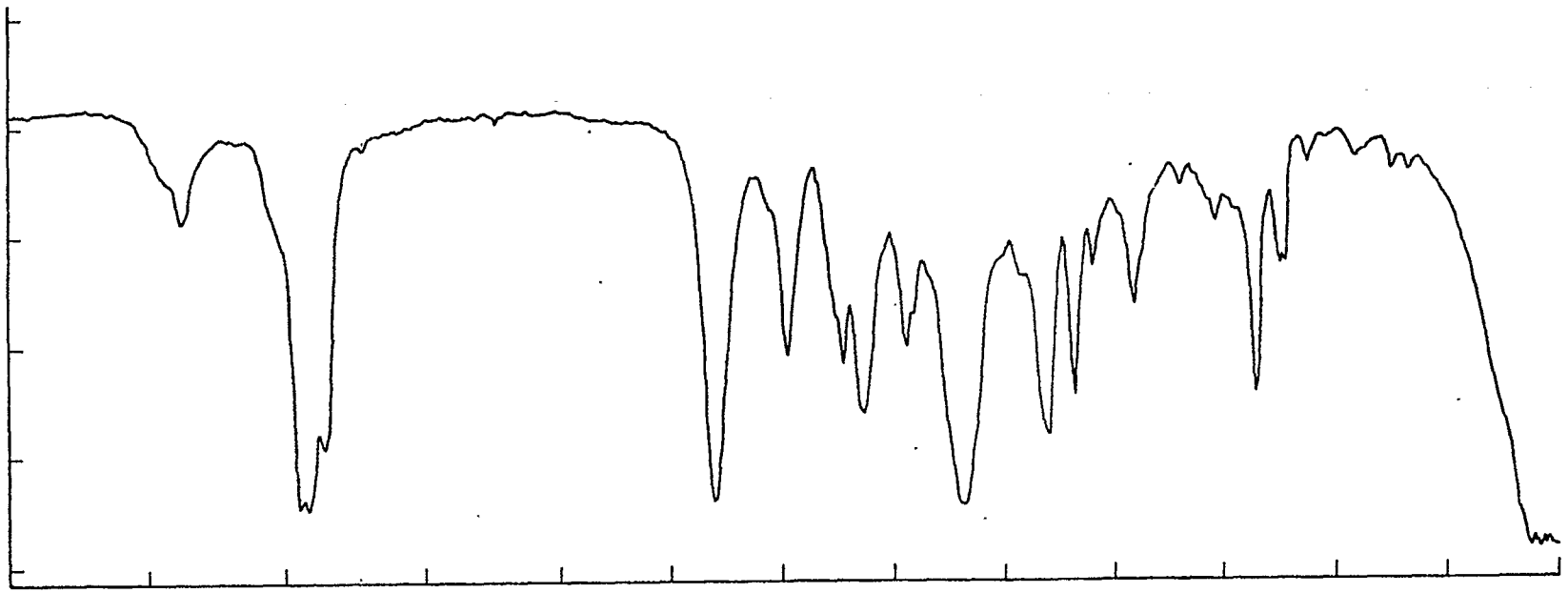

Figure 4. Hiawatha CDL, Fraction #2, Phenyl μ-Bondapak column.
IR: 283 Perkin-Elmer in % Transmission mode.

Task 3

Catalysis and Mechanism of Coal Liquefaction

Catalytic Action of Zinc Chloride in Short-Residence Coal Hydrogenation

Faculty Advisor: David M. Bodily
Graduate Student: Tsejung Ray

Introduction

Metal halides such as $ZnCl_2$ are well-known to be active catalysts for coal hydrogenation. Zinc chloride has been shown to be a very effective catalyst for coal hydrogenation in the entrained-flow reactor developed at the University of Utah.[1,2] Bell and co-workers[3-5] have studied the reactions of model compounds with $ZnCl_2$ under conditions similar to those employed in coal hydrogenation. They observed cleavage of C-O and C-C bonds in the model compound and proposed that the active catalytic species is a Bronsted acid formed from $ZnCl_2$.

Shibaoka, Russell and Bodily[6] proposed a model to explain the liquefaction of coal, based on microscopic examination of the solid products from metal halide catalyzed coal hydrogenation. The model involves a competition between hydrogenation and carbonization reactions. The hydrogenation process starts at the surface of vitrinite particles and progresses toward the center. The vitrinite is converted to a plastic material of lower reflectance, which is the source of oils, asphaltenes and preasphaltenes. Concurrently, carbonization occurs in the center of the particles, resulting in vesiculation and a higher reflectance material. The partially carbonized material can be hydrogenated at later stages, but at a lower rate than the original coal.

Thermal and/or catalytic bond rupture occurs during the liquefaction process. The initial products of the bond cleavage reactions may be stabilized by hydrogen addition, resulting in cleavage of bridges between aromatic ring systems and in dealkylation of aromatic rings. If the initial products of the reaction are not stabilized, they may polymerize to form semicoke-like material. This primary semicoke may be isotropic or exhibit a fine-grained anisotropic mosiac texture, depending on the rank of the coal. The plastic material formed by stabilization of the initial products may be further hydrogenated or, under hydrogen deficient conditions, may form secondary semicoke. The secondary semicoke is of medium to course-grained anisotropic mosiac texture. Bodily and Shibaoka[7] used this model to explain the nature of the residues from hydrogenation in the short-residence, entrained-flow hydrogenation reactor. The role of the $ZnCl_2$ catalyst is examined in this study.

Project Status

A reactor system has been constructed to hydrogenate coals at short-residence times. The reactor consists of a short length of high-pressure tubing connected by pressure fittings to a pressure gauge and valve. The

coal sample will be introduced into the reactor and the system pressurized with hydrogen. The reactor is connected to a vibrator to provide agitation of the sample and mixing with the hydrogen. The reactor will be lowered into a heated fluidized sand bath bringing the coal sample quickly to reaction temperature. The reactor will be removed from the bath after the reaction to quench the reaction.

Future Work

The reactor will be used to hydrogenate coal with $ZnCl_2$ catalyst at various temperatures. The effect of $ZnCl_2$ on the softening temperature of the coal will be quantitatively determined.

References

1. R.E. Wood and W.H. Wiser, Ind. Eng. Chem., Proc. Design Devel., 15, 144 (1976).

2. J.M. Lytle, R.E. Wood and W.H. Wiser, Fuel, 59, 471 (1980).

3. D.P. Mobley and A.T. Bell, Fuel, 58, 661 (1979).

4. N.D. Taylor and A.T. Bell, Fuel, 59, 499 (1980).

5. D.P. Mobley and A.T. Bell, Fuel, 59, 507 (1980).

6. M Shibaoka, N.J. Russell and D.M. Bodily, Fuel, submitted.

7. D.M. Bodily and M. Shibaoka, Fuel, submitted.

Task 5

The Mechanism of Pyrolysis of Bituminous Coal

Faculty Advisor: W.H. Wiser
Graduate Student: J.K. Shigley

Introduction

In the present state of knowledge concerning the fundamental chemistry of coal liquefaction in the temperature range 375-550° C, the liquefaction reactions are initiated by thermal rupture of bonds in the bridges joining configurations in the coal, yielding free radicals. The different approaches to liquefaction, except for Fischer-Tropsch variations, represent ways of stabilizing the free radicals to produce molecules. The stabilization involving abstraction by the free radicals of hydrogen from the hydroaromatic structures of the coal is believed to be the predominant means of yielding liquid size molecules in the early stages of all coal liquefaction processes, except Fischer-Tropsch variations. The objective of this research is to understand the chemistry of this pyrolytic operation using model compounds which contain structures believed to be prominant in bituminous coals.

Project Status

Experiments have been conducted with test mixtures of carbazole and benzene or toluene. The inability to obtain material balances at different helium flowrates seems to suggest that a problem exists with the injection technique. Also analysis inconsistencies (i.e., peak tailing, peak broadening, peak ghosting) suggested that problems may be occurring with the 1/8" column. Several 1/4" columns have been tested to determine if this would solve some of the problems.

Future Work

The system[1] will be reconfigured so as to correct the problems with the injection technique. The new injection technique will utilize the 4-port Valco switching valve to interrupt the carrier gas flow from the gas chromatograph and utilize helium flow from the system for a short injection period, then switching back to the gas chromatographic carrier gas flow. Experiments will be conducted with carbazole and benzene or toluene, with varying helium flow rates through the system and with the 1/4" chromatographic columns.

Reference

1. W.H. Wiser, J.K. Shigley, DOE Contract No. DE-AC22-79ET14700, Quarterly Progress Report, Salt Lake City, Utah, April-June 1981.

Task 6

Catalytic Hydrogenation of CD Liquids and Related Polycyclic Aromatic Hydrocarbons

Faculty Advisor: J. Shabtai
Research Associate: C. Russell

Introduction

The main objective of this research project is to develop a versatile process for controllable hydrotreating of highly aromatic coal liquids, viz., a process permitting production of naphthenic-aromatic feedstocks containing variable relative concentrations of hydroaromatic vs. aromatic ring structures. Such feedstocks, including the extreme case of a fully hydrogenated coal liquid, are suitable starting materials for catalytic cracking, as applied for preferential production of light liquid fuels. The overall objective of this project and of a parallel catalytic cracking study is, therefore, to develop and optimize a hydrotreating-catalytic cracking process sequence for conversion of coal liquids into conventional fuels.

The present project includes also a study of metal sulfide-catalyzed hydrogenation of model polycyclic arenes present in coal liquids, e.g., phenanthrene, pyrene, anthracene and triphenylene, as a function of catalyst type and experimental variables. This part of the study provides basic information on the rate, mechanism and stereochemistry of hydrogenation of structurally distinct aromatic systems in the presence of sulfided catalysts.

Project Status

This report provides results obtained in a kinetic study of the hydrogenation of pyrene (1) in the presence of a sulfided Ni-W/Al_2O_3 catalyst (precursor: Nalco Sphericat 550). Hydrogenation experiments were carried out in an autoclave system described elsewhere[1], and modified to allow for collection of samples during the reaction. Products were identified by a combination of gas chromatography and mass spectrometry, and in some cases also by comparison with pure reference compounds.

Kinetic rate constants were obtained for a reaction pressure of 2500 psig, at reaction temperatures of 300° and 350°C. Figures 1 and 2 show the changes in product composition from hydrogenation of pyrene as a function of reaction time at 300° and 350°C, respectively. Figure 3 indicates the proposed reaction network for hydrogenation of pyrene, along with the kinetic rate constants determined in this study.

Figure 3 indicates three alternative initial products formed in the hydrogenation of pyrene, i.e., 4,5-dihydropyrene (2); 1,2,3,3a,4,5-hexahydropyrene (4) and 1,2,3,6,7,8-hexahydropyrene (3). The kinetic analysis showed that neither 3 nor 4 were formed by hydrogenation of 2, but that these compounds were formed instead by hydrogenation of 1. Consequently, it is postulated that both 3 and 4 are formed via a highly reactive intermediate, i.e., 1,2-dihydropyrene (1a), obtained by

hydrogenation of 1, and having a partially quinonoid structure. Further, the kinetic analysis showed that the rate of consumption of 1 by hydrogenation was greater than the sum of the rate constants for formation of 2, 3 and 4 from 1. This indicated that some of the reacting pyrene remained on the catalyst as a condensed product which is designated in Figure 3 as coke. Rate constants in Figure 3 show that this coke formation increases markedly with temperature. A possible consequence of this coke formation is seen in the rate constants k_4, k_7 and k_8, which decrease with an increase in temperature. This indicates some deactivation of the active sites for those reactions.

The results in Figure 3 indicate that for intermediate compounds with two or three hydrogenated rings, e.g., compounds 4, 6 and 7, the subsequent hydrogenation step involves preferentially a trisubstituted rather than a tetrasubstituted aromatic ring. Thus, the intermediate 4 undergoes faster hydrogenation to 6 than to 7 ($k_7 > k_8$ both at 300° and 350°C). Likewise, hydrogenation of the residual tetrasubstituted ring in 6 to yield 8 is considerably slower as compared to the hydrogenation of the residual trisubstituted ring in 7 to yield 8 ($k_{11} > k_{10}$, especially at 350°C). The latter observation is consistent with the anticipated higher steric interference (of the hydroaromatic rings) with flatwise adsorption of the residual aromatic ring in 6 as compared with that in 7.

Future Work

Kinetic studies of the hydrogenation of chrysene, naphthacene and dibenzochrysene will be initiated. A kinetic study using SRC-II distillate fractions as hydrogenation feeds will also be carried out.

Reference

1. L. Veluswamy, Ph.D. Thesis, University of Utah, Salt Lake City, Utah, 1977.

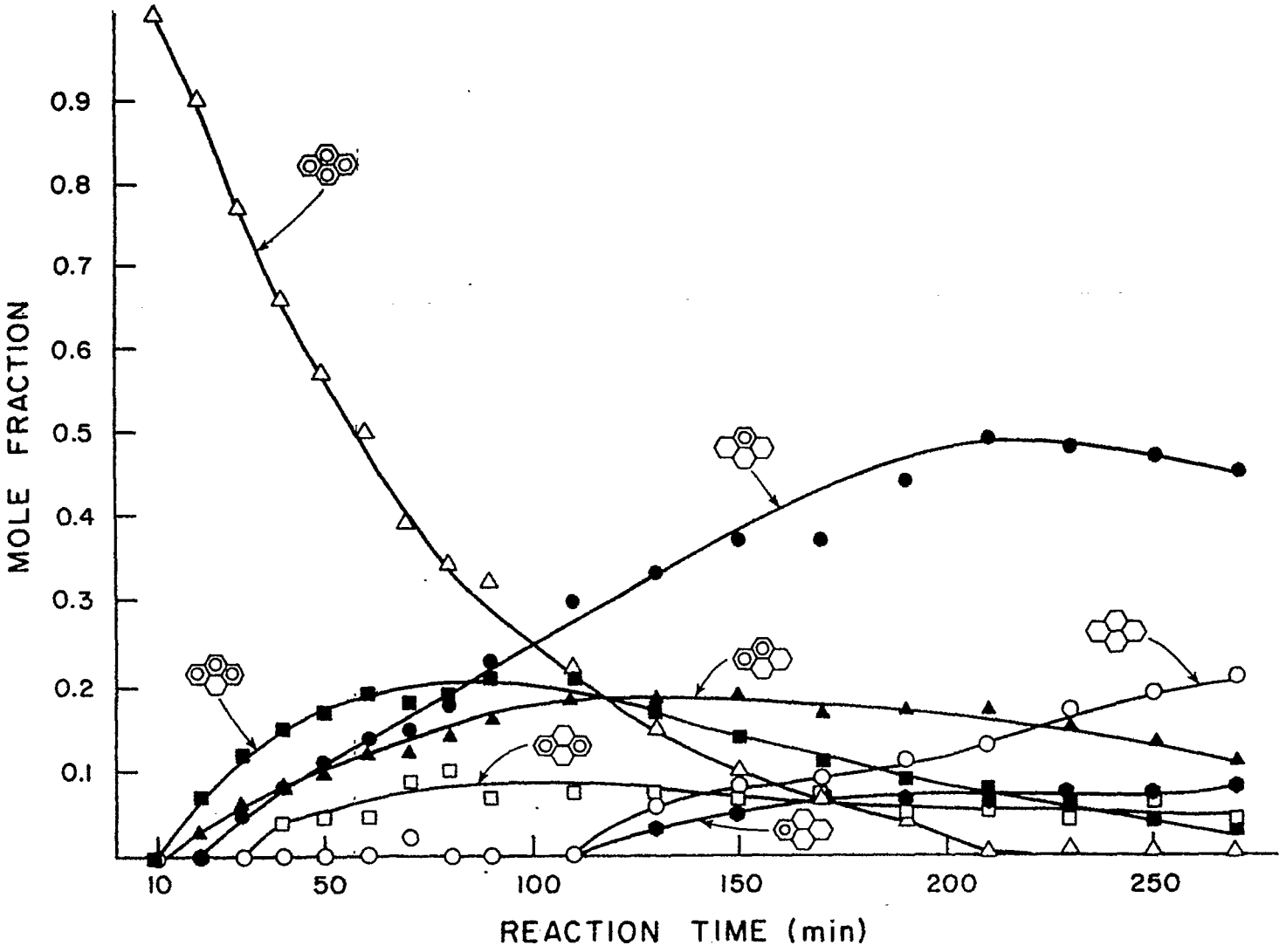

Figure 1. Change in product composition from hydrogenation of Pyrene as a function of reaction. Catalyst: sulfided Ni-W/Al_2O_3; Pressure: 2500 psi; Temperature: 300°C.

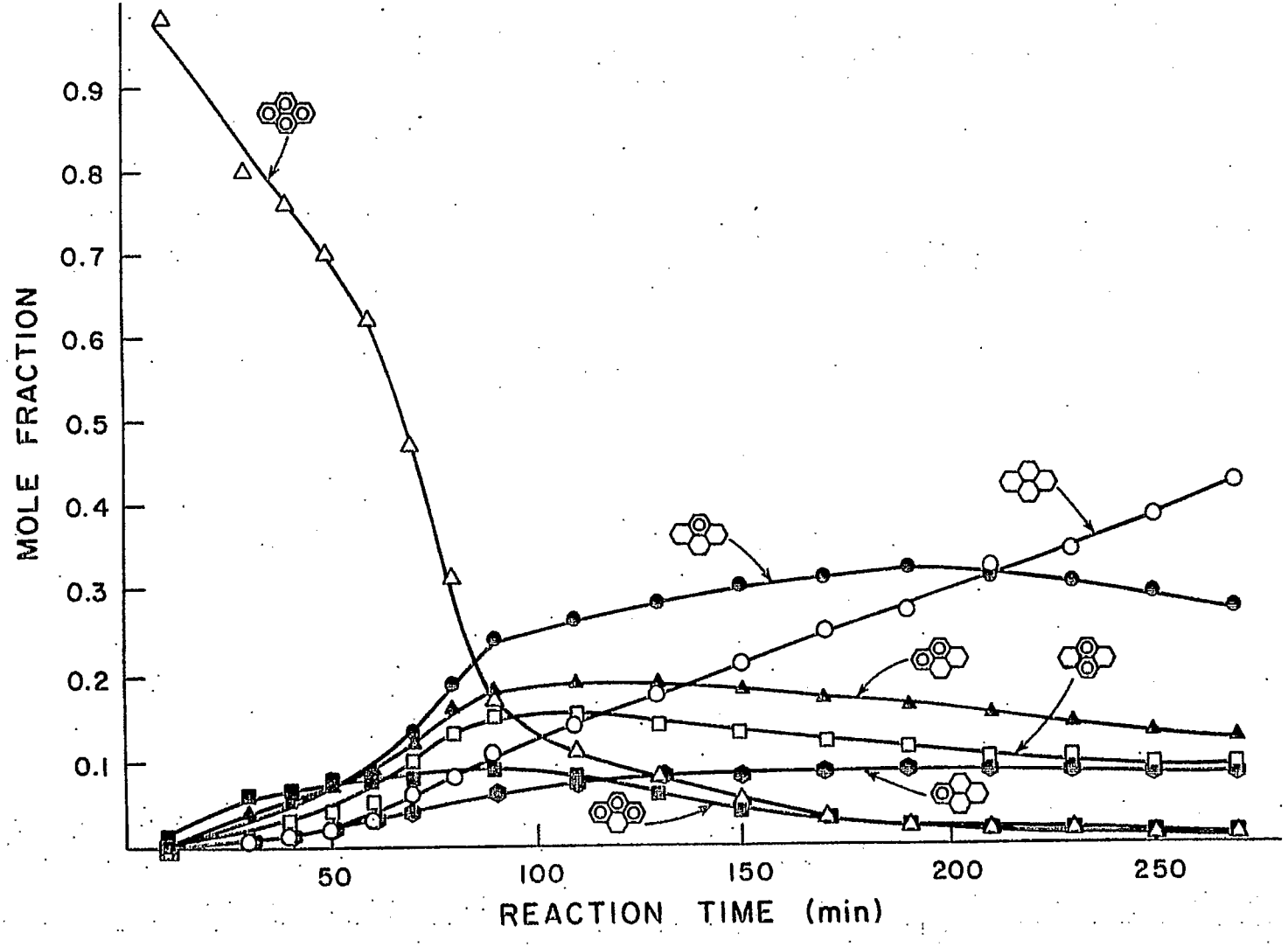

Figure 2. Change in product composition from hydrogenation of Pyrene as a function of time. Catalyst: sulfided Ni-W/Al_2O_3; Pressure: 2500 psi; Temperature: 350°C.

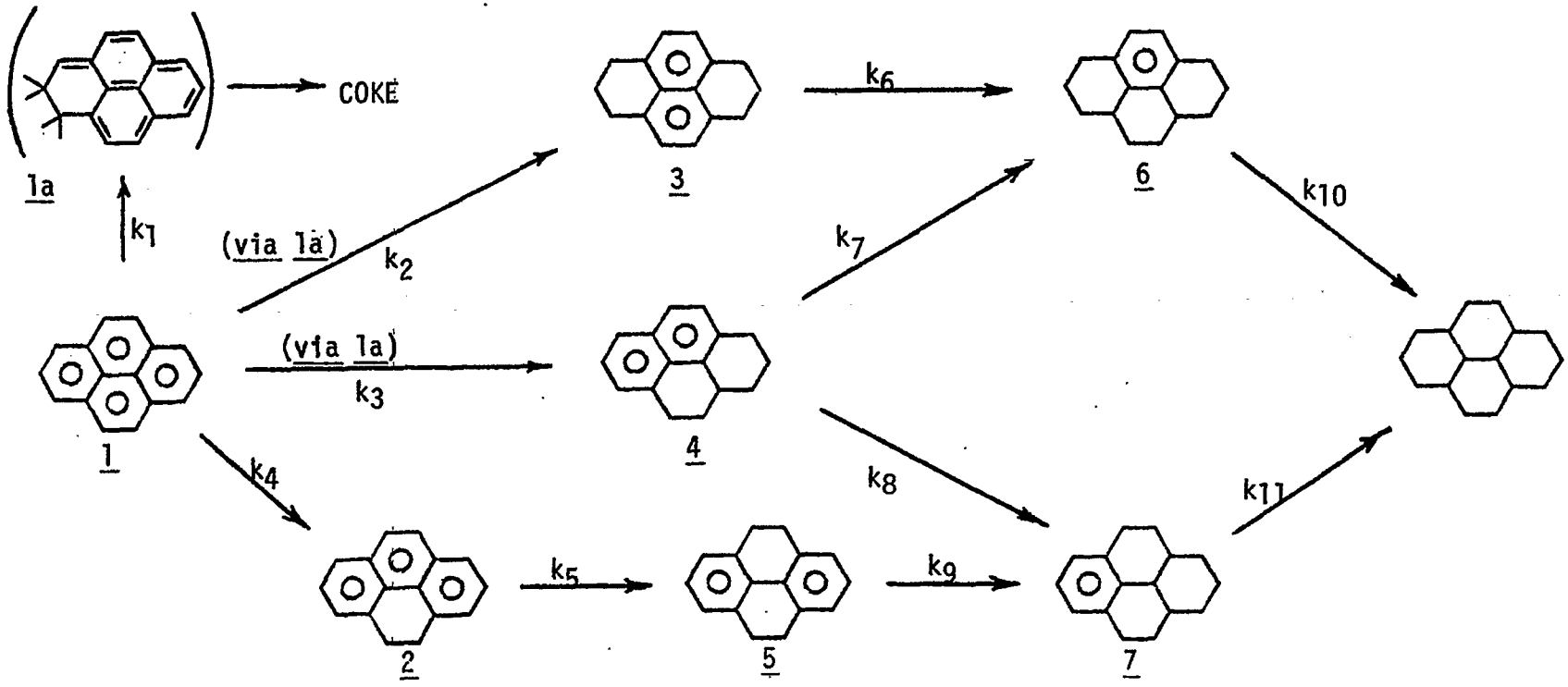

Figure 3. Hydrogenation of Pyrene--Reaction Network
Rate Constants, min^{-1} (Pressure: 2500 psig; catalyst: sulfided Ni-W/Al_2O_3).

T, °C	k_1	k_2	k_3	k_4	k_5	k_6	k_7	k_8	k_9	k_{10}	k_{11}
300	0.005	---	0.003	0.007	0.012	---	0.0027	0.0022	0.036	0.003	0.007
350	0.20	0.0033	0.0039	0.003	---	0.0039	0.0020	0.0015	---	<0.001	0.019

Task 7

Denitrogenation and Deoxygenation of CD Liquids and Related N- and O- Compounds

Catalytic Hydrodeoxygenation of Coal-Derived Liquids and Related Oxygen-Containing Compounds

Faculty Advisors: J. Shabtai
A.G. Oblad
Graduate Student: G. Haider

Introduction

Coal-derived liquids are characterized by the presence of a considerable concentration of oxygen-containing components. Therefore, a systematic catalytic hydrodeoxygenation (HDO) study of coal-derived liquids and related model compounds is being carried out. The study provides information not only on the mechanism of HDO as related to catalytic upgrading of coal liquids, but also on the role of oxygen-containing compounds in primary coal liquefaction processes.

Project Status

At present, coal liquefaction processes which bear the potential of commercialization operate under severe reaction conditions, e.g., temperature: 425-475°C; hydrogen pressure: 1500-2500 psig; reaction time: 30-60 min. In such processes, e.g., SRC-I, SRC-II and EDS, etc., coal liquefaction involves partial heteroatom (S, N and O) removal. Catalytic upgrading of coal-derived liquids (CDL) is accompanied by further elimination of such heteroatoms. It was of interest to examine the relative ease of N, S and O extrusion from CDL in the presence of conventional sulfided catalysts. Since oxygen-containing functional groups play an important role as linkage groups in the coal framework, it was also of considerable interest to determine the relative ease of hydrodeoxygenative elimination of various chemically distinct types of groups. Therefore, in this part of the study the hydrogenation-hydrodeoxygenation of a CDL product was systematically investigated as a function of reaction temperature (200-370°C) and catalyst type. An SRC-II distillate, b.p. 230-455°C, was used as feedstock, and sulfided Co-Mo/Al_2O_3 and Ni-W/Al_2O_3 as catalysts. Experiments were performed in a semi-batch autoclave reactor and products obtained were examined by a combination of elemental analysis, and detailed infrared and C^{13}NMR analyses.

The present report provides data on the change in elemental composition of HDO products from the above indicated SRC-II distillate as a function of temperature and catalyst type. Results of the IR and C^{13}NMR studies will be reported in subsequent reports.

Table 21 summarizes data on the change in elemental composition of HDO products obtained from the SRC-II distillate, using sulfided Co-Mo/Al_2O_3 as catalyst. Table 22 and Figure 29 on the other hand summarize the change in residual heteroatom content on a weight percentage basis. As seen, the extent of heteroatom removal increases with increase in reaction temperature. Sulfur is essentially completely eliminated at 370°C. Nitrogen is more difficult to remove (residual content, 9.1% at

370°C). Figure 30 (see also Table 21) shows the observed change in hydrogen content and H/C atomic ratio of the HDO products as a function of reaction temperature. As seen, the hydrogen content increases with increase in reaction temperature up to a maximum near 320°C (hydrogen content, 9.6%; H/C atomic ratio, 1.30). Above 350°C, however, there is a gradual decrease in the hydrogen content, as well as in the H/C atomic ratio. This may be due to the anticipated increase in the extent of dealkylation reactions, as well as to displacement of the aromatic ring hydrogenation-dehydrogenation equilibria in the direction of dehydrogenation at these high temperatures (vide infra, C^{13}NMR data).

Table 23 summarizes the change in elemental composition of HDO products obtained from SRC-II distillate, using sulfided Ni-W/Al_2O_3 as catalyst. Table 24 and Figure 31 show the change in residual heteroatom (N,S and O) content in the HDO products, on a weight percentage basis. As seen, the heteroatom removal increases with increase in reaction temperature. Sulfur is almost completely removed at 350°C. As with the sulfided Co-Mo catalyst, nitrogen is more difficult to eliminate (residual content, 6.8% at 370°C), while oxygen extrusion is the most difficult (residual content, 24.6% at 370°C). Figure 32 shows the observed change in hydrogen content and H/C atomic ratio of the HDO products as a function of temperature. As seen, the hydrogen content increases with increase in temperature up to a maximum near 350°C (hydrogen content, 10%; H/C ratio, 1.35). Above 350°C, however, as with sulfided Co-Mo/Al_2O_3 catalyst, the hydrogen content decreases (vide supra).

Comparison of Figure 29 with Figure 31 indicates that at 230-350°C the Co-Mo catalyst is somewhat more effective for oxygen removal, viz., it has higher C-O hydrogenolysis activity as compared to the sulfided Ni-W catalyst. Further, comparison of Figure 30 and Figure 32 indicates that the hydrogen uptake during hydrotreatment of the SRC-II distillate is consistently higher with the Ni-W catalyst as compared with the Co-Mo catalyst. In other words, hydrotreatment with the Ni-W system is associated with higher hydrogen consumption per hetero gram atom removed. This behavior is clearly related to the higher ring hydrogenation activity of the Ni-W as compared to the Co-Mo catalyst system (see preceding reports).

TABLE 21

CHANGE IN ELEMENTAL ANALYSIS OF PRODUCTS FROM HYDRODEOXYGENATION OF SRC-II (MIDDLE-HEAVY DISTILLATE, b.p. 230 - 455°C) AS A FUNCTION OF REACTION TEMPERATURE[a-e] (SULFIDED Co-Mo CATALYST)

Reaction Temperature, °C	Content, % b. wt.					H/C Atomic Ratio
	C	H	N	S	O	
Feed	86.14	8.23	2.20	0.40	3.03	1.15
200	86.80	8.31	1.72	0.24	2.97	1.15
230	87.76	8.51	1.32	0.21	2.20	1.16
260	88.08	8.66	1.16	0.10	2.00	1.18
290	88.31	8.98	1.11	0.07	1.53	1.22
320	88.23	9.60	0.72	0.05	1.40	1.30
350	89.24	9.46	0.39	0.03	0.88	1.27
370	89.72	9.35	0.20	< 0.01	0.73	1.25

(a) For characteristic properties of SRC-II middle-heavy distillate, see Tables 30 and 31; (b) In each experiment were used 10 g. of feed and 2 g. of catalyst; (c) Catalyst, Co-Mo/Al_2O_3 (Nalco 471, for composition see Table 28); the catalyst was sulfided prior to use (see Experimntal); (d) Hydrogen pressure, 1750 psig; (e) Total reaction time, 1 hr.

TABLE 22

CHANGE IN RESIDUAL HETEROATOM CONTENT OF PRODUCTS FROM HYDRODEOXYGENATION OF SRC-II (MIDDLE-HEAVY DISTILLATE, b.p. 230 - 455°C) AS A FUNCTION OF REACTION TEMPERATURE[a-e] (SULFIDED Co-Mo CATALYST)

Reaction Temperature, °C	Residual Heteroatom Content, % by wt.		
	N	S	O
200	78.2	60.0	98.0
230	60.0	52.5	72.6
260	52.7	25.0	66.0
290	50.5	17.5	50.5
320	32.7	12.5	46.2
350	17.7	7.5	29.0
370	9.1	< 0.1	24.1

(a) For characteristic properties of SRC-II middle-heavy distillate, see Tables 30 and 31; (b) In each experiment were used 10 g. of feed and 2 g. of catalyst; (c) Catalyst, Co-Mo/Al_2O_3 (Nalco 471, for composition see Table 28); the catalyst was sulfided prior to use (see Experimental); (d) Hydrogen pressure, 1750 psig; (e) Total reaction time, 1 hr.

TABLE 23

CHANGE IN ELEMENTAL ANALYSIS OF PRODUCTS FROM HYDRODEOXYGENATION OF SRC-II (MIDDLE-HEAVY DISTILLATE, b.p. 230 - 455°C) AS A FUNCTION OF REACTION TEMPERATURE[a-e] (SULFIDED Ni-W CATALYST)

Reaction Temperature, °C	Content, % b. wt.					H/C Atomic Ratio
	C	H	N	S	O	
Feed	86.14	8.23	2.20	0.40	3.03	1.15
230	87.81	8.68	1.19	0.13	2.19	1.19
260	87.85	8.90	1.09	0.06	2.10	1.22
290	88.12	9.35	0.81	0.02	1.70	1.27
320	88.27	9.80	0.46	0.01	1.46	1.33
350	88.57	10.00	0.35	< 0.01	1.08	1.35
370	89.51	9.60	0.15	< 0.01	0.74	1.29

(a) For characteristic properties of SRC-II middle-heavy distillate, see Tables 30 and 31; (b) In each experiment were used 10 g. of feed and 2 g. of catalyst; (c) Catalyst, Ni-W/Al_2O_3 (Sphericat 550, for composition see Table 28); the catalyst was sulfided prior to use (see Experimental); (d) Hydrogen pressure, 1750 psig; (e) Total reaction time, 1 hr.

TABLE 24

CHANGE IN RESIDUAL HETEROATOM CONTENT OF PRODUCTS FROM HYDRODEOXYGENATION OF SRC-II (MIDDLE-HEAVY DISTILLATE, b.p., 230 - 455°C) AS A FUNCTION OF REACTION TEMPERATURE[a-e] (SULFIDED Ni-W CATALYST)

Reaction Temperature, °C	Residual Heteroatom Content, % by wt.		
	N	S	O
230	54.1	32.5	72.3
260	49.5	15.0	69.3
290	36.8	5.0	56.1
320	20.9	2.5	48.2
350	15.9	< 0.1	36.6
370	6.8	< 0.1	24.4

(a) For characteristic properties of SRC-II middle-heavy distillate, see Tables 30 and 31; (b) In each experiment were used 10 g. of feed and 2 g. of catalyst; (c) Catalyst, Ni-W/Al_2O_3 (Sphericat 550, for composition see Table 28); the catalyst was sulfided prior to use (see Experimental); (d) Hydrogen pressure, 1750 psig; (e) Total reaction time, 1 hr.

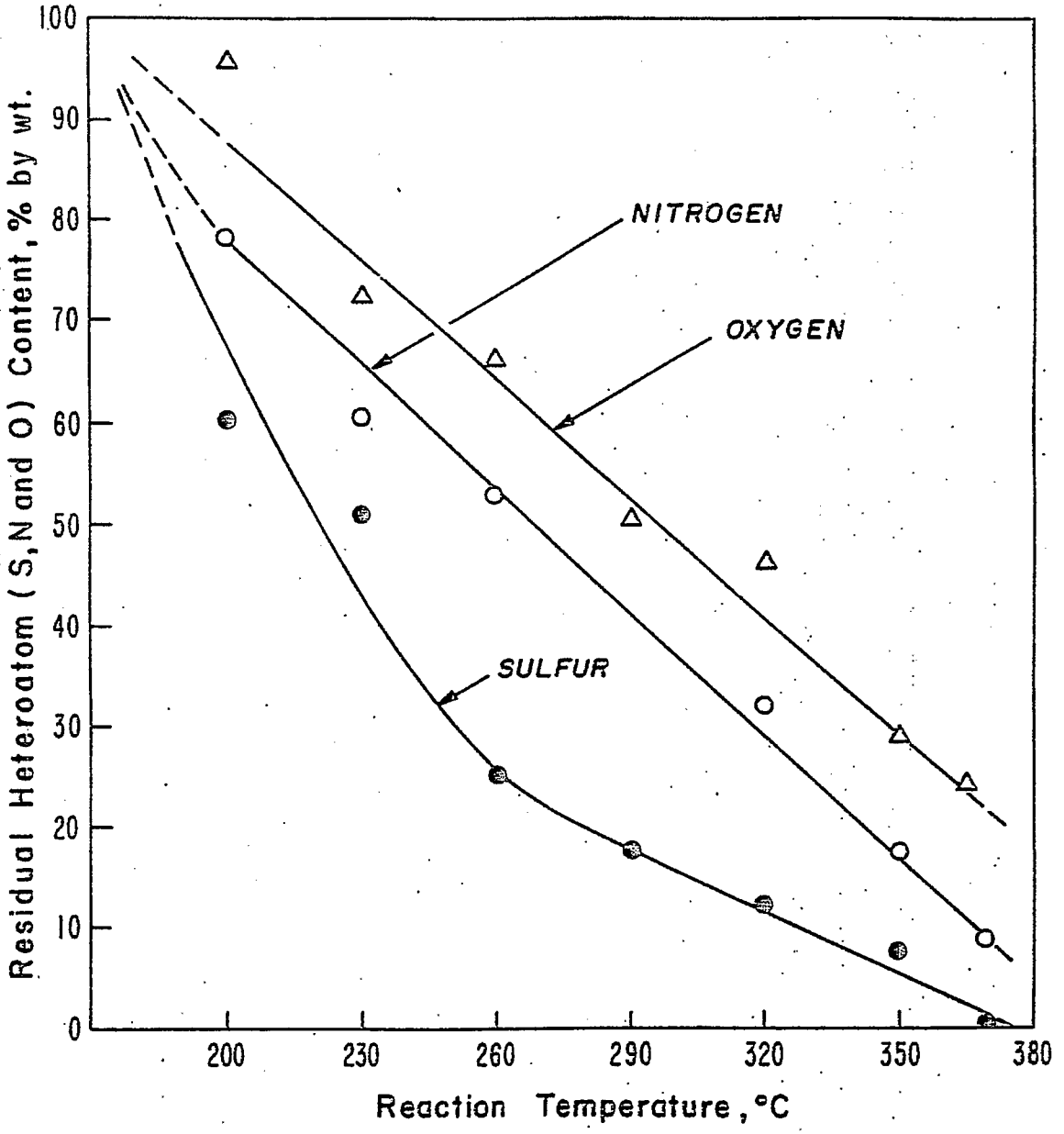

Figure 29. Change in Residual Heteroatom Content in Product from Hydrogenation of SRC-II Distillate (b.p. 230 - 455°C) as a Function of Reaction Temperature (Hydrogen Pressure: 1750 psig; Reaction Time: 1 hr.; Catalyst: Sulfided Co-Mo/Al_2O_3).

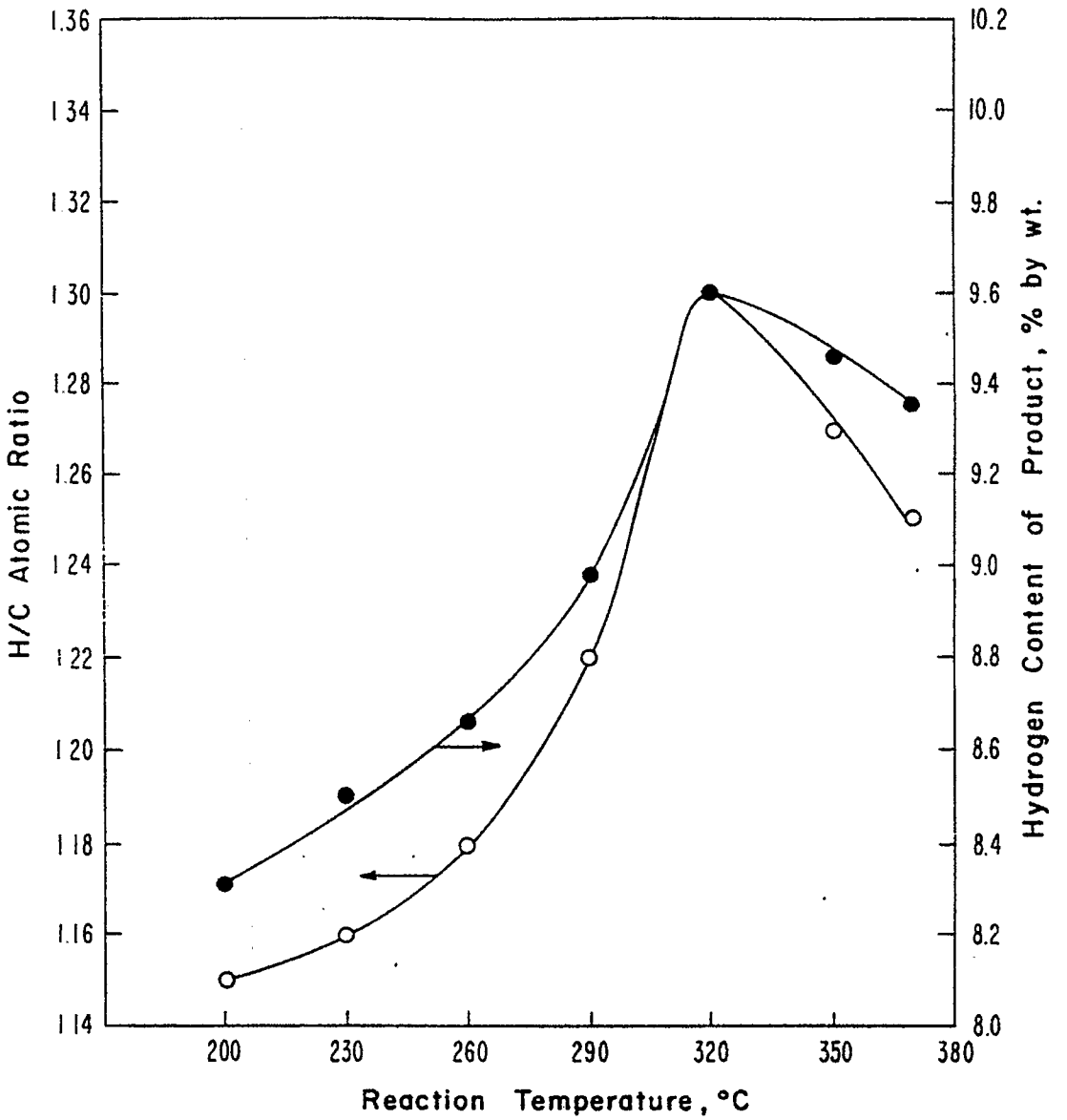

Figure 30. Change in Hydrogen Content and H/C Atomic Ratio of Product from Hydrodeoxygenation of SRC-II Distillate (b.p. 230 - 455°C) as a Function of Reaction Temperature (Hydrogen Pressure: 1750 psig; Reaction Time: 1 hr.; Catalyst: Sulfided Co-Mo/Al_2O_3).

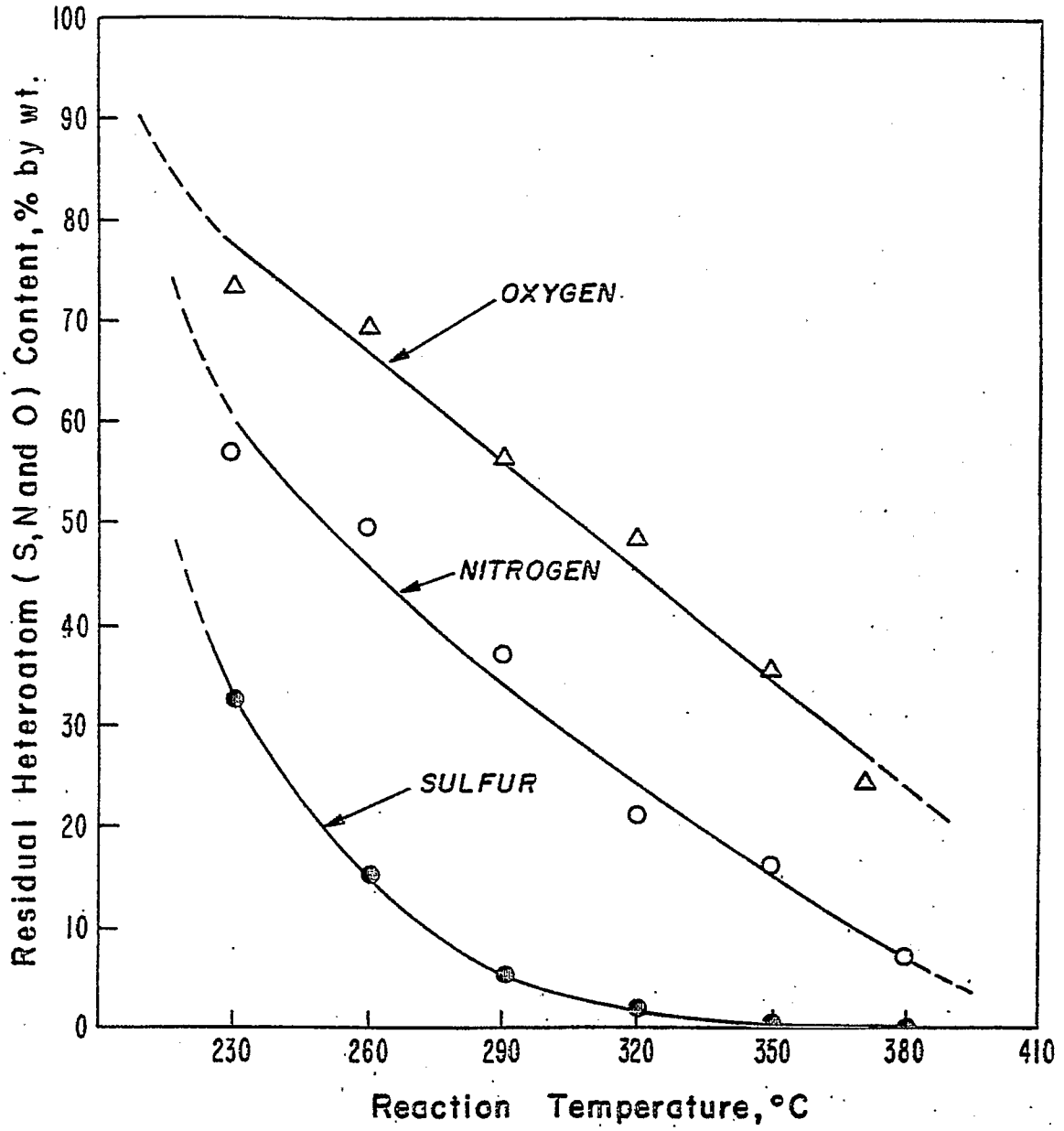

Figure 31. Change in Residual Heteroatom Content in Product from Hydrogenation of SRC-II Distillate (b.p. 230 - 455°C) as a Function of Reaction Temperature (Hydrogen Pressure: 1750 psig; Reaction Time: 1 hr.; Catalyst: Sulfided Ni-W/Al_2O_3).

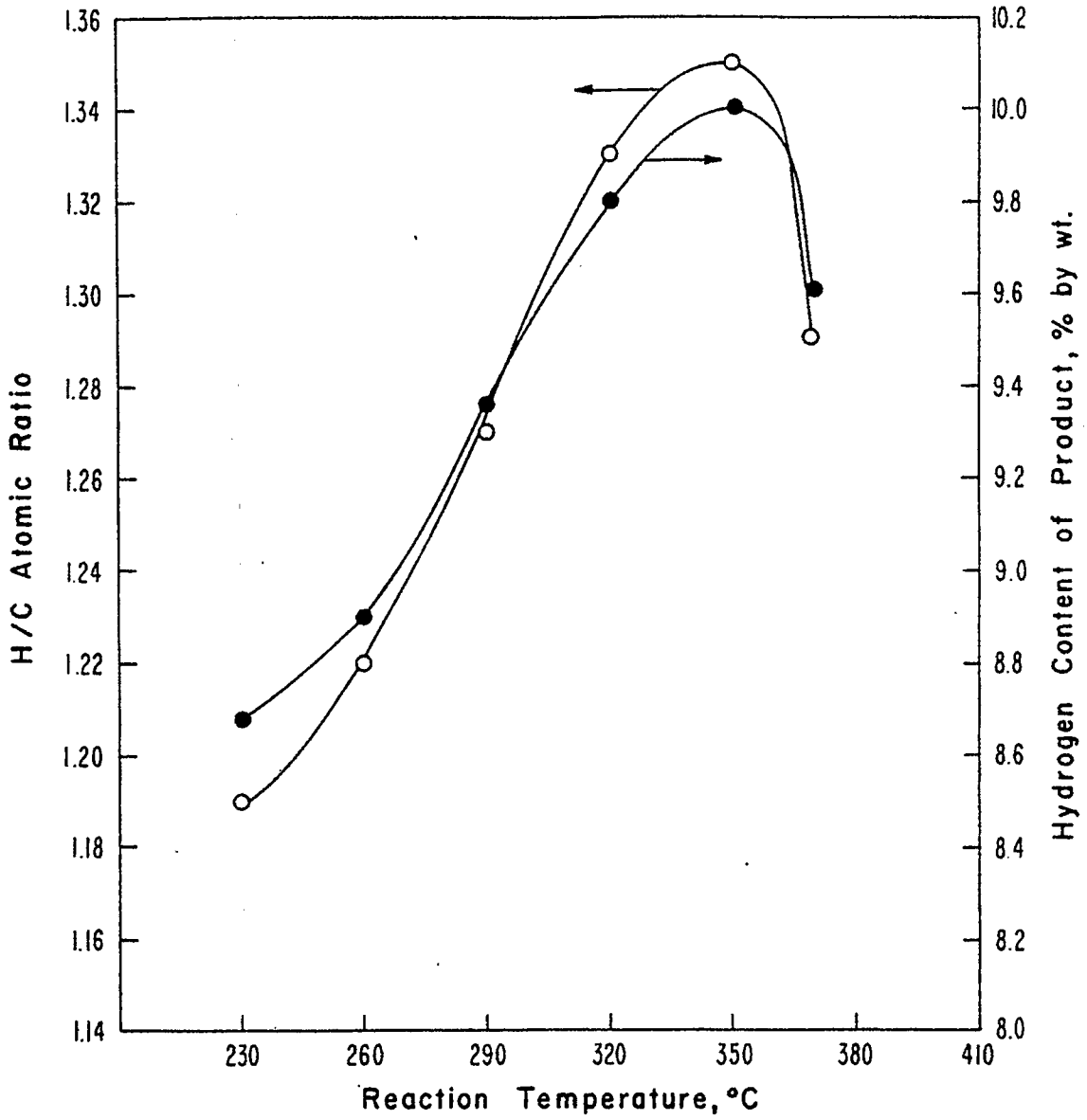

Figure 32. Change in Hydrogen Content and H/C Atomic Ratio of Product from Hydrodeoxygenation of SRC-II Distillate (b.p. 230 - 455°C) as a Function of Reaction Temperature (Hydrogen Pressure: 1750 psig; Reaction Time: 1 hr.; Catalyst: Sulfided Ni-W/Al_2O_3).

Task 8

Catalytic Cracking of Hydrogenated Coal-Derived Liquids and Related Compounds

Faculty Advisors: J. Shabtai
A.G. Oblad
Graduate Student: Z. Pai

Introduction

Hydrogenation followed by catalytic cracking provides a feasible process sequence for conversion of coal liquids into conventional fuels. Such a sequence has certain advantages in comparison with a hydrocracking-catalytic reforming scheme.

The present project is concerned with the following interrelated subjects: (1) systematic catalytic cracking studies of polycyclic naphthenes and naphthenoaromatics found in hydrogenated coal liquids and (2) systematic catalytic cracking studies of hydrotreated coal-derived liquids.

Project Status

Work on the preparation of (a) partially hydrogenated SRC-I extracts and (b) partially hydrogenated polycyclic arenes (see DE/ET/14700-7) was continued during July 1981. In August 1981, the graduate student performing Task 8 took a 1 1/2 months leave of absence without pay for personal reasons. The research work will be resumed upon his return.

Future Work

Catalytic cracking studies with the above indicated types of partially hydrogenated feedstocks will be continued.

Task 9

Hydropyrolysis (Thermal Hydrocracking) of CD Liquids

Faculty Advisors: J. Shabtai
A.G. Oblad
Graduate Student: Y. Wen

Introduction

This project is concerned with a systematic investigation of hydropyrolysis (thermal hydrocracking) as an alternative processing concept for upgrading of heavy coal-derived liquids into light liquid products. The high efficiency and versatility of hydropyrolysis has been indicated in previous studies with heavy CDL feedstocks and with model compounds.[1-3] The present project is an extension of this previous work for the purpose of (a) further developing and enlarging the scope of the hydropyrolytic reaction, and (b) optimizing the operating conditions for different types of feedstocks, e.g., coal liquids from different liquefaction processes, partially hydrotreated coal liquids, and relevant model compounds. The project includes systematic studies of reaction kinetics, product composition, and coking tendencies, as a function of operating variables. The work with model compounds provides necessary data for further elucidation of mechanistic aspects of the hydropyrolysis process.

Project Status

The construction of the new hydropyrolysis unit (see DE/ET/14700-6) was completed. Testing of the reactor, using mildly hydrotreated SRC-II products and tetralin as feeds, was initiated in August 1981.

Future Work

Hydropyrolysis studies with the above indicated types of feedstocks will be continued.

References

1. J. Shabtai, R. Ramakrishnan and A.G. Oblad, Advances in Chemistry, No. 183, Thermal Hydrocarbon Chemistry, Amer. Chem. Soc., 1979, pp 297-328.

2. R. Ramakrishnan, Ph.D. Thesis, University of Utah, Salt Lake City, Utah, 1978.

3. A.G. Oblad, J. Shabtai and R. Ramakrishnan, pending patents.

Task 10

Systematic Structural Activity Study of Supported Sulfide Catalysts for Coal Liquids Upgrading

Faculty Advisors: F.E. Massoth
J. Shabtai
Post-Doctoral Fellows: G. Muralidhar
Y. Liu

Introduction

The objective of this research is to develop an insight into the basic properties of supported sulfide catalysts and to determine how these relate to coal liquids upgrading. The proposed program involves a fundamental study of the relationship between the surface-structural properties of various supported sulfide catalysts and their catalytic activities for various types of reactions. Thus, there are two clearly defined and closely related areas of investigation, viz., (1) catalyst characterization, especially of the sulfided and reaction states and (2) elucidation of the mode of interaction between catalyst surfaces and organic substrates of different types. The study of subject (1) will provide basic data on sulfided catalyst structure and functionality, and would allow the development of catalyst surface models. Subject (2), on the other hand, involves systematic studies of model reactions on sulfide catalysts, and the utilization of data obtained for development of molecular level surface reaction models correlating the geometry (and topography) of catalyst surfaces with the steric-conformational structure of adsorbed organic reactants. The overall objective of the project is to provide fundamental data needed for design of specific and more effective catalysts for upgrading of coal liquids.

Atmospheric activity tests using model compounds representative of hydrodesulfurization (thiophene), hydrogenation (hexene) and cracking (isooctene) have been developed. These were employed to assay changes in the catalytic functions of various supported CoMo catalysts. It was found that hydrodesulfurization (HDS) and hydrogenation activities were generally unaffected by the type of alumina used or by the cobalt salt used in the preparation; whereas, cracking activity varied considerably, being highest for γ-Al_2O_3 and cobalt sulfate addition. Addition of acidic, basic or neutral ions to the standard γ-alumina catalyst at 0.5 wt % level showed interesting changes in catalytic activities for various functions. In a series of catalysts employing silica-alumina as the support, the HDS and hydrogenation functions decreased with increasing silica content, while cracking went through a maximum in activity. Catalysts prepared by supporting CoMo on TiO_2, SiO_2·MgO and carbon showed low activities, except for high cracking activity for the two former catalysts.

Project Status

During this quarter, a SiO_2·Al_2O_3 series of catalysts containing Mo was prepared and evaluated to compare with previous results on the same series containing CoMo. Catalysts of both series in the calcined

precursor state were examined by ESCA.

Catalytic activity results for thiophene HDS and hexene hydrogenation for the Mo containing catalysts are given in Table 1. Because of the lower activity of these catalysts compared to the CoMo series, the reactions were carried out at 400°C instead of 350°C previously employed. Activity trends for this series were quite similar to the CoMo series,[1] viz., (1) a rapid decline in HDS activity followed by a slower loss with increasing SiO_2 content of the support, (2) a more gradual and approximately linear decrease in hydrogenation activity with increasing SiO_2. X-Ray examination of the calcined catalysts showed the appearance of crystalline MoO_3 at SiO_2 levels above 25% SiO_2. The decrease in catalytic activity can be attributed to poorer dispersion of the Mo phase.

ESCA measurements were carried out on the same series as well as the series with CoMo. These measurements were done on the calcined catalysts since the dry box attachment to the ESCA instrument to allow in situ examination of sulfided catalyst is not yet complete. Measurements on the supports themselves were also made for calibration purposes. Catalyst samples were ground to a fine powder and dusted onto double stick tape. Integrated areas of the relevant peaks were determined by a computer coupled to the ESCA instrument. The surface dispersion of the elements of interest were calculated using the following equations:[2]

$$\delta_i = F_i \frac{I_j/I_j^0}{\sum_1^j I_j/I_j}$$

$$F_i = \left[\frac{W_{Al} r_{Al} + W_{Si} r_{Si}}{r_i}\right]^{3/2}$$

where δ is the surface dispersion, F the matrix factor, I the peak intensity, I^0 the peak intensity in an appropriate reference compound, W the weight fraction, r the ionic radius, and subscripts i, j, Al and Si refer to elements i, j, alumina and silica. Surface dispersions for Al_2O_3 and SiO_2 calculated with the above formulas showed the proper linear correlations with catalyst composition, attesting to the validity of the calculations.

Variation in the Mo dispersion as a function of SiO_2 content in the silica-alumina support is presented in Figure 1. Both catalyst series show a similar trend in decreasing dispersion with increase in SiO_2 content. This decrease can be attributed to a weaker interaction between the Mo phase and the support, as evidenced by the decrease in the peak half-width values of Table 1.

Figure 2 shows the relationship between catalytic activities for HDS and hydrogenation versus Mo dispersion relative to the Al_2O_3 catalyst. An approximate linear correlation obtains for hydrogenation, but HDS falls significantly below the linear correlation line. These results indicate that hydrogenation sites are decreasing proportionally with a decrease in Mo dispersion in the surface, whereas HDS sites are decreasing faster. The difference in response is in agreement with previous findings that different sites are involved for the two reactions.[3] The presence of Co does not seem to affect the results greatly, indicating that the promotional role of Co is about the same for all catalysts.

Assembly of the high pressure reactor for catalyst screening tests has been completed and runs should start during the next period. Difficulty has been experienced with the pressure seal on the stirred tank reactor. While this is being fixed, the preheater will be used as a fixed bed reactor so that preliminary catalyst testing can be undertaken.

Future Work

ESCA work on Si-Mg and TiO_2 supported oxide catalysts and also on selected sulfided catalysts will be undertaken. Standard cobalt molybdenum catalysts, containg various additives at a 5% level, will be prepared and tested. Sulfur analyses on molybdenum supported on silica-alumina series will also be carried out.

References

1. W.H. Wiser, F.E. Massoth, J. Shabtai and G. Muralidhar, DOE Contract No. DE-AC01-79ET14700, Quarterly Progress Report, Salt Lake City, Utah, Apr-June, 1980.

2. M.P. Seah, Suf. Interface Anal., Vol. 2, No. 6 (1980).

3. R. Ramchandran and F.E. Massoth, J. Catal., 67, 248 (1981)

Table 1. Characterization results for Mo-SiO_2-Al_2O_3 catalysts.

Catalyst[a]	Rate Constants[b] k_T	k_H	X-Ray Anal.[c]	XPS FWHM (ev)
γ-Al_2O_3	4.2	49.2	-	2.4
10% SiO_2	2.5	43.2	-	2.2
25% SiO_2	1.5	37.7	MoO_3(w)	2.2
75% SiO_2	1.3	27.7	MoO_3(m)	1.8
SiO_2	1.0	23.2	MoO_3(s)	1.9

[a] All catalysts contained 8% Mo on the support.

[b] k_T for HDS, k_H for hydrogenation.

[c] Oxide precursor state.

FIGURE 1

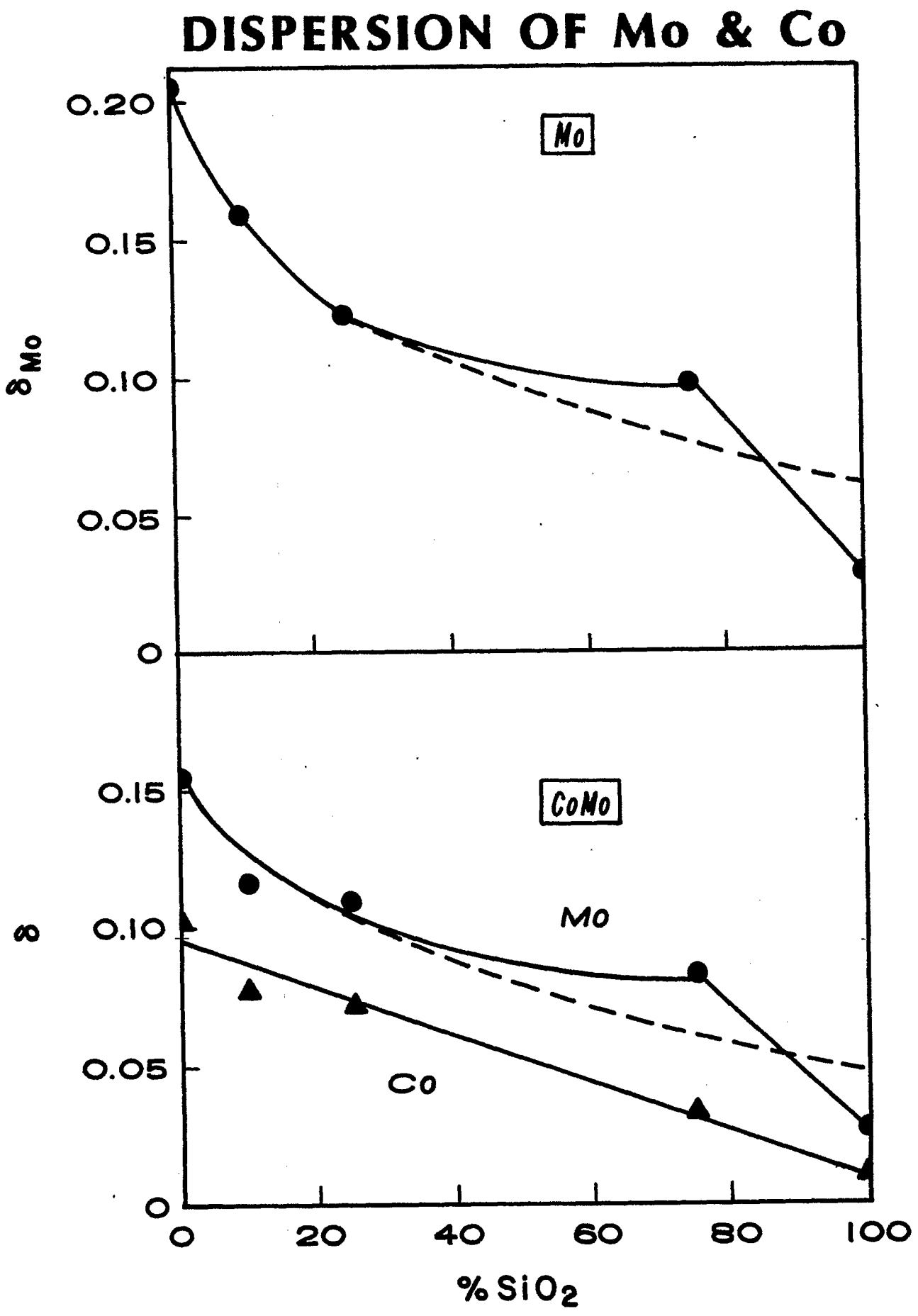
DISPERSION OF Mo & Co
Mo
CoMo
Mo
Co
δ_{Mo}
δ
0.20
0.15
0.10
0.05
0
0.15
0.10
0.05
0
0
20
40
60
80
100
% SiO_2

FIGURE 2

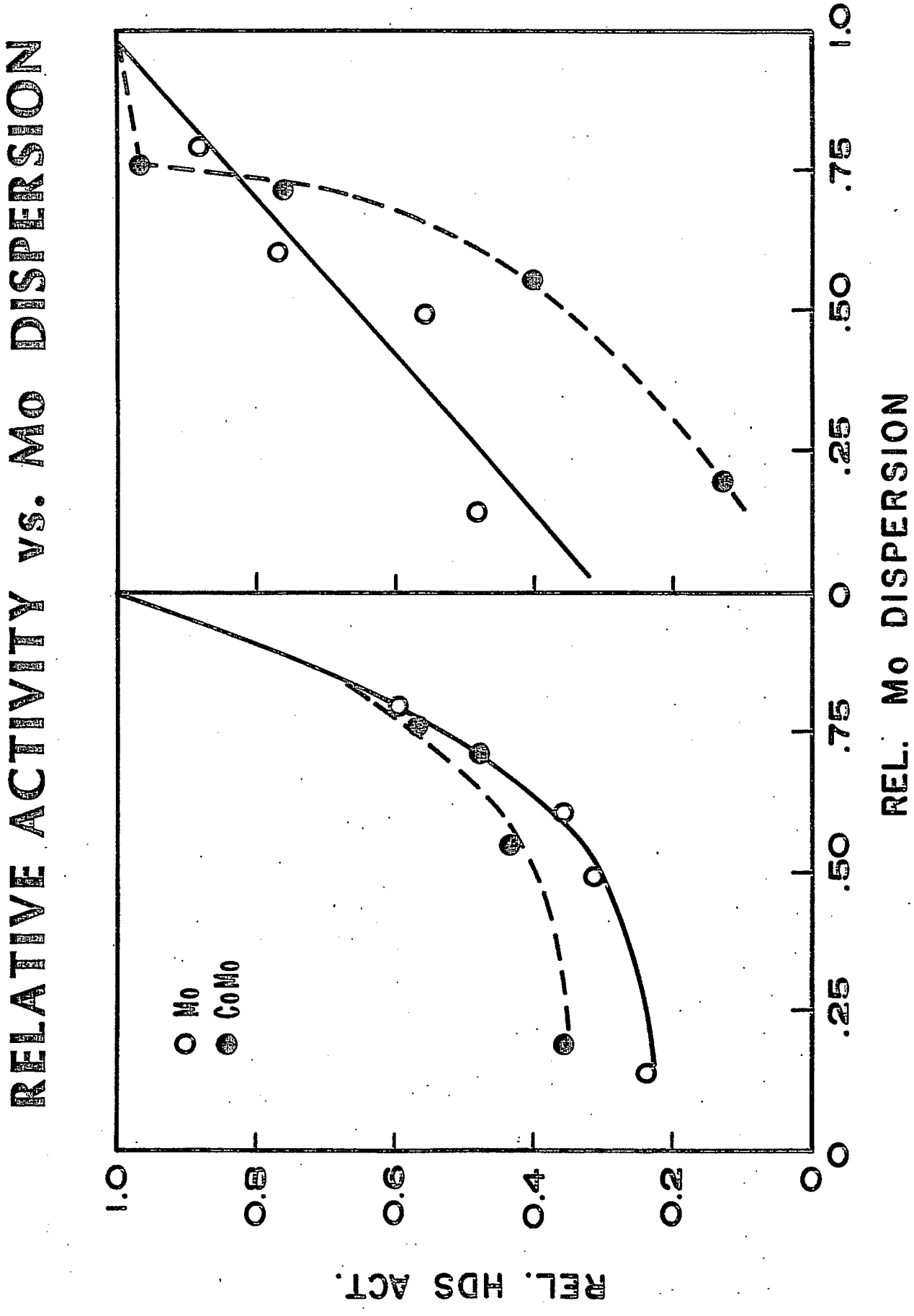
RELATIVE ACTIVITY vs. Mo DISPERSION
REL. HDS ACT.
REL. Mo DISPERSION
Mo
CoMo
0
0.2
0.4
0.6
0.8
1.0
.25
.50
.75

Task 11

Basic Study of the Effects of Poisons on the Activity of Upgrading Catalysts

Faculty Advisor: F.E. Massoth
Post-Doctoral Fellow: W. Zmierczak

Introduction

The importance of cobalt-molybdena catalysts for hydrotreating and hydrodesulfurization of petroleum feedstocks is well-known. These catalysts are also being studied for hydrodesulfurization and liquefaction of coal slurries and coal-derived liquids. However, such complex feedstocks result in rapid deactivation of the catalysts. To gain an insight into the deactivation mechanism, the detailed kinetics of reactions of model compounds representative of heteratom hydrogenolysis and hydrogenation are compared before and after addition of various poisons and coke precursors. The studies are carried out using a constant stirred microbalance reactor, which enables simultaneous measurement of catalyst weight change and activity. Supplementary studies are made to gain additional insight into the effect of poisons on the active catalyst sites. Finally, catalysts aged in an actual coal pilot plant run are studied to compare with laboratory studies.

Previous work on this project has shown that catalyst poisoning by pyridine or coke results in loss of active HDS sites, but that the remaining unpoisoned sites retain their original activity. Pyridine appeared to be site selective in poisoning effect whereas coke was non-specific. Furthermore, a distribution of HDS site strengths was observed with pyridine poisoning.

Project Status

Last quarter, the use of oxygen chemisorption for quantitatively assessing the number of active sites on HDS catalysts was investigated. It was found that O_2 adsorption on the sulfided catalyst was only reliable at -78°C, oxidation occurring at higher adsorption temperatures. Furthermore, Mo/Al_2O_3 and $CoMo/Al_2O_3$ catalysts gave essentially the same O_2 adsorption, despite the fact that the latter catalyst has a much greater HDS activity. Apparently the Co promotion on HDS is not accounted for in the O_2 adsorption measurements. To establish whether the method would be suitable to characterize catalysts containing both Co and Mo, a number of catalysts which had previously been evaluated for catalytic activity under Task 10 were subjected to O_2 chemisorption.

Catalytic properties of the CoMo catalysts (3% Co, 8% Mo on different supports) were described earlier.[1,2] Experimental data were obtained using a flow microbalance reactor.[3] The catalyst was contained in a gold mesh bucket surrounded by the reactor volume space and suspended from one arm of an electrobalance. Before O_2 adsorption, the catalyst was heated overnight, sulfided for four hours in a 10% H_2S/H_2 gas mixture flow, followed by two hours in helium. Then, the reactor temperature was lowered to -78°C (dry ice-acetone bath). Oxygen was adsorbed from 5% air in helium mixture for several hours to obtain equilibrium. After this, physically adsorbed O_2 was removed in a helium flow. The O_2 adsorption data for the various catalysts

is given in Table 1. Figure 1 shows correlations between HDS activity or hydrogenation activity and O_2 adsorption. Both catalytic functions roughly correlate with O_2 adsorption, despite differences in the two functions for the different catalysts. That is, the data scatter do not allow distinguishing between a direct correlation of adsorption with HDS or hydrogenation activities with certainty. However, correlation for hydrogenation appears to be better (R^2=0.88) than for HDS (R^2=0.74); the greater data scatter in the latter could be due to differences in the Co promotion in the different catalysts. Correlation with hydrogenation activity could be a significant finding but more data are needed to confirm this. It should be mentioned that some workers have reported a correlation with HDS activity[4] while others with hydrogenation activity[5] on a limited number of catalysts. Adsorption of O_2 is believed to take place preferentially on edge sites of the basic MoS_2 crystallites.[6] If this is true, then the present results would appear to indicate that hydrogenation occurs at these sites rather than HDS, since it has been demonstrated that the sites are different for these two reactions.[7]

The effect of pyridine poisoning on oxygen chemisorption capacity has also been carried out. In these experiments, a commerical catalyst, American Cyanamid 1442 A (3% Co, 8% Mo/Al_2O_3), was used. The catalyst was heated overnight at 400°C in He, sulfided for four hours in 10% H_2S/H_2 gas mixture, followed by two hours in helium. Then the reactor temperature was lowered to 350°C and the catalyst was treated with a He stream saturated with pyridine at 0°C for varying time intervals. Oxygen chemisorption was performed as described above. The results are shown in Figure 2. A linear decrease in O_2 adsorption with increasing preadsorbed pyridine was obtained. In the range 0-15 mg pyridine/g, the decline in HDS activity for benzothiophene was previously investigated on a different but similar catalyst.[8] In the latter case, a curvature in the activity-pyridine weight plot was obtained, in contrast to the linear O_2 adsorption plot of Figure 2. The different responses would appear to indicate a lack of correlation between O_2 adsorption and HDS activity, although the use of different catalysts in the two cases and the presence of coke on the catalyst in the activity measurements (see below) make this conclusion tenuous at present.

To assess whether the O_2 chemisorption technique would give valid results on catalysts after they had been used in reaction studies, the following experiment was performed on a $CoMo/Al_2O_3$ catalyst. After sulfiding as before, the temperature was lowered to 350°C and a stream of thiophene in H_2 was passed over the catalyst for an overnight period. A weight gain of about 2 mg/g was experienced during this period, indicating some coking of the catalyst. Chemisorption of O_2 at -78°C was then carried out as before. The results showed that a constant amount of O_2 was not adsorbed, but rather the catalyst weight increased rapidly and then continued to increase with time. The continued uptake is most likely due to adsorption of O_2 on the coke, making it difficult to accurately determine the O_2 chemisorbed on the active catalyst sites. Similar results were obtained on a Mo/Al_2O_3 catalyst. These results would appear to invalidate the method for reacted and coked catalysts, contrary to limited findings of Tauster and Riley.[9]

Future Work

Adsorption experiments to develop a convenient technique for measuring

active sites on cobalt molybdate catalysts will continue. If successful, this technique will be utilized to measure residual active sites and effects of specific poisons on the kinetics of various catalytic functions on these catalysts. A stirred microbalance reactor will be used for the poisoning studies using N-containing organic bases of different strengths to assess strengths and numbers of active HDS sites.

References

1. W.H. Wiser, F.E. Massoth, J. Shabtai and G. Muralidhar, DOE Contract No. DE-AC01-79Et14700, April - June 1980.

2. ibid., Jan - Mar 1981.

3. F.E. Massoth, Chemtech, May 1972, p. 285.

4. S.J. Tauster and K.L. Riley, J. Catal., 67, 250 (1981).

5. V. Vyskocil and D. Tomanova, React. Kinet. Catal. Lett., 10, 37 (1979).

6. S.J. Tauster, T.A. Pecoraro and R.R. Chianelli, J. Catal., 63, 515 (1980).

7. R. Ramachandran and F.E. Massoth, J. Catal., 67, 248 (1981).

8. W.H. Wiser, F.E. Massoth and R. Ramachandran, DOE Contract No. DE-AC01-79ET14700, Apr-June 1980.

9. S.J. Tauster, T.A. Pecoraro and R.R. Chianelli, J. Catal., 63, 515 (1980).

Table 1. Oxygen Chemisorption Capacity for Different Co-Mo Catalysts.

Catalyst Support	Oxygen Chemisorption Capacity (mg/g)
100% γ-Al_2O_3	0.75
10% SiO_2, 90% Al_2O_3	0.56
25% SiO_2, 75% Al_2O_3	0.59
75% SiO_2, 25% Al_2O_3	0.36
100% SiO_2	0.11
SiO_2 MgO	0.47
TiO_2	0.13

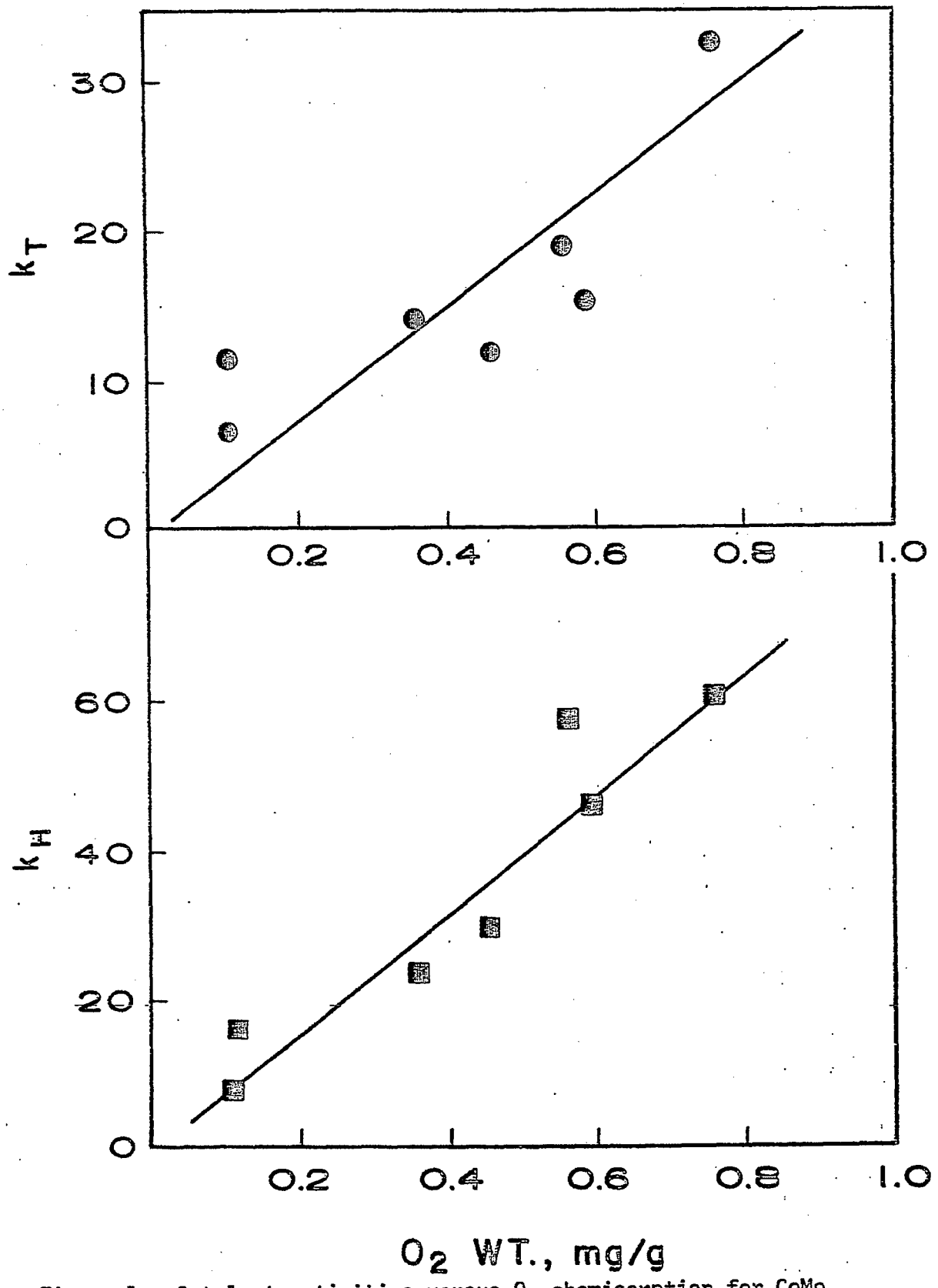

Figure 1. Catalyst activities versus O_2 chemisorption for CoMo on various supports. k_t and k_H are rate constants for thiophene HDS and hexene hydrogenation, respectively.

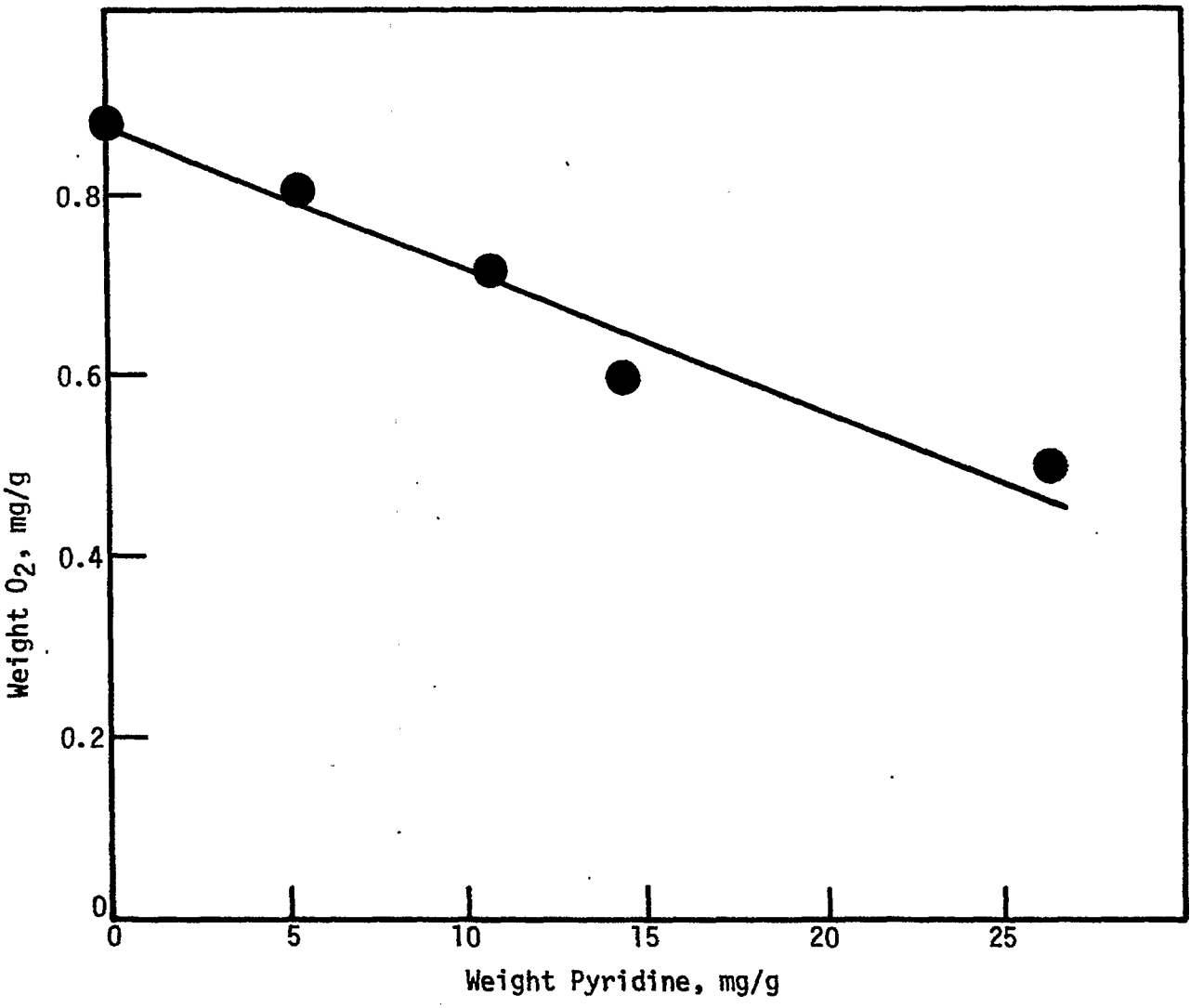

Figure 2. Effect of preadsorbed pyridine on O_2 chemisorption.

Task 12

Diffusion of Polyaromatic Compounds in Amorphous Catalysts Supports

Faculty Advisor: F.E. Massoth
Graduate Student: A. Chantong

Introduction

This project involves assessing diffusional resistances within amorphous-type catalysts. Of primary concern is the question of whether the larger, multiring hydro-aromatics found in coal-derived liquids will have adequate accessibility to the active sites within the pores of typical processing catalysts. When molecular dimensions approach pore size diameters, the effectiveness of a particular catalyst is reduced owing to significant mass transport resistance. An extreme case occurs when molecular and pore size are equivalent, and pores below this size are physically inaccessible.

The project objective can be achieved through a systematic study of the effect of molecular size on sorptive diffusion rates relative to pore geometry. Conceptually, the diffusion of model aromatic compounds is carried out using a stirred batch reactor. The preferential uptake of the aromatic from the aliphatic solvent is measured using a UV spectrometer. Adsorption isotherms are determined to supplement the diffusion studies.

Initial work entailed development of a suitable reactor, measurement techniques and methods of data analysis. These demonstrated that adsorption was diffusion-controlled. In the early studies, effective diffusivities were larger than predicted for pore diffusion and a surface diffusion contribution was postulated. Subsequent studies, using improved techniques, gave effective diffusivities equal to or lower than predicted, casting doubt on the validity of surface diffusion in our system. The lower values were obtained with larger solute molecules and smaller catalyst pore sizes. A correlation was developed relating a drag coefficient to the ratio of the solute to pore size.

Project Status

Diffusion runs with tetra-phenylporphine and alumina C were carried out in three different solvents, namely cyclohexane, hexane and heptane. The experiments were carried out to check the effect of solvent on pore diffusion coefficients.

Satterfield and Cheng[1,2] found that steric hindrance from solvent molecules significantly reduced the diffusion coefficient of the solute in zeolite pores. It was shown that diffusion rates of solutes diffusing into initially empty pores of a NaY zeolite were orders of magnitude faster than solutes diffused into the initially solvent filled pores. Solute-solvent interactions were also found to have a large effect on diffusion rate of the solute. The diffusion coefficient of cumene in NaY zeolite with cyclohexane as the solvent was found to be about two orders of magni-

tude larger than that when benzene was used as the solvent. Caro et al.[3] studied the sorptive diffusion of n-decane in single crystals of 5A zeolite from a nonadsorbing liquid solvent (molecules too large to enter the zeolitic micropores). Cyclohexane, ethylbenzene, and butylbenzene were used as solvents. The sorptive diffusion rate of n-decane in 5A zeolite was found to decrease as the solvent molecular size increased. The rate decreased in the order cyclohexane > ethylbenzene > butylbenzene. This was explained by blocking effects caused by solvent molecules interacting with the outer zeolite crystal surface.

Table 1 shows measured effective diffusion coefficients for tetraphenylporphine in alumina C with cyclohexane, hexane and heptane as solvents. The effective diffusion coefficient is seen to be dependent on the solvent and in line with bulk diffusivities of the solute in the three solvents. The ratios of effective to bulk diffusivities are constant. Therefore, the effect of solvent on the pore diffusion is due to the difference in the bulk diffusivities of the solute in the solvents and not to any intrinsic effect on pore diffusion.

Unlike diffusion in zeolites, no solvent effect was observed with alumina. Because of the extremely small pore sizes in zeolites compared to solvent molecular sizes, a small change in molecular size of the solvent could have a significant effect on the diffusion rate. In our system, pore sizes in the alumina are large compared to the solvent molecular sizes, and therefore, steric hindrance or blocking effects caused by small changes in solvent molecular size are not observed.

Normally, in diffusion studies of activated carbon, a single resistance diffusion model (macropore diffusion) has been used in treating the data. But some investigators[4,5] have found that sorptive diffusion in activated carbons was controlled by the combined effects of both macropore and micropore diffusion. Dawazoe and Takevchi[4] studied diffusion of Kr-85 in activated carbon. They considered the pore size distribution of the activated carbon to be bimodal. The carbon particles were pictured as an aggregate of minute spherical particles consisting of macropores between the particles and micropores within them. Diffusion within the particles was assumed to be in series with macropore diffusion. Peel et al.[5] showed that the single resistance diffusion model did not fully describe the sorptive diffusion kinetics in activated carbon due to the wide range of pore sizes. The pore size distribution was divided into two regions, namely macropores and micropores. The micropores were assumed to be homogenously distributed throughout the particle and to branch off the larger macropore network, which was responsible for radial transport. The model was shown to fit the sorptive diffusion data of phenols in activated carbon better than the single resistance diffusion model.

By varying particle size, the rate-limiting transport process can be determined. If micropore transport is rate limiting, the uptake rate due to sorptive diffusion as a function of time should be independent of particle size. If macropore transport is rate-limiting, the uptake rate should be proportional to the inverse of the square of the particle radius. Where both micropore and macropore diffusion are important, intermediate behavior is expected.[4]

The aluminas used in the present study have a considerable range of pore sizes. Diffusion runs with different particle sizes were carried out to check the effect of the pore size distribution. Figure 1 shows

the uptake rate plots of three different particle sizes. The uptake rate is clearly shown to be dependent on particle size. A plot of uptake vs. t/R^2 is shown in Figure 2. It can be seen that the uptake is inversely proportional to the square of the particle radius. This shows that macropore diffusion is rate-limiting. Also, as shown in Table 2, the diffusion coefficients (which include R^2 in the calculations) for the three different particle sizes are in good agreement. Even though the alumina has a wide range of pore sizes, the single resistance model seems to adequately describe the adsorptive diffusion process in this system.

A sample of alumina exhibiting a bimodal pore-size distribution was obtained from the Pittsburgh Energy Technology Center.[6] The pore size distribution is shown in Figure 3. The alumina has two different average pore sizes, 150 Å and 1700 Å. Diffusion runs with tetraphenylporphine/cyclohexane with this alumina were carried out to check the effect of the bimodal pore structure. Table 3 shows the pore diffusion coefficients for two different particle sizes obtained from using the single resistance diffusion model. The diffusion coefficients from the two particle sizes show good agreement. The single resistance diffusion model also seems to be applicable to the sorptive diffusion in this bimodal alumina.

Future Work

This phase of the project has been completed and a Ph.D. thesis will be written on the work accomplished. When another student becomes available, the project will continue. Future work will involve diffusion measurements at elevated temperatures and pressures to develop correlation relationships with model compounds and with narrow fraction cuts of coal liquids.

References

1. C.N. Satterfield and C.S. Cheng, AIChE Journal, 18, 724 (1972).
2. C.N. Satterfield and C.S. Cheng, Chem. Eng. Prog. Symp. Ser., 67 (117), 43 (1972).
3. J. Caro, M. Bulow and J. Kargen, AIChE Journal, 26, 1044 (1972).
4. K. Kawazoe and Y. Takevchi, J. of Chem. of Japan, 7, 431 (1974).
5. R.G. Peel, A. Benedek and C.M. Crowe, AIChE Journal, 27, 26 (1981).
6. Courtesy of Dr. H. Appel.

Table 1. Effective diffusivities of tetraphenylporphine in different solvents with alumina C.

Solvent	Diffusion Coefficient Bulk, D_b† $cm^2/sec \times 10^6$	Diffusion Coefficient Effective, D_e $cm^2/sec \times 10^6$	Ratios D_e/D_b
cyclohexane	4.37	1.61	0.37
heptane	11.0	4.59	0.42
hexane	13.0	4.84	0.37

†Calculated from Wilke-Chang equation.

Table 2. Pore diffusion coefficient of tetraphenylporphine in cyclohexane with different particle sizes of alumina D.

Particle Mesh Size	Particle Radius (cm)	$D_{p_2} \times 10^6$ cm^2/sec
+60-100	0.0099	1.28
+35-65	0.01575	1.21
+24-35	0.02815	1.27

Table 3. Pore diffusion coefficient of tetraphenylporphine in cyclohexane with bimodal alumina.

Particle Mesh Size	Final Concentration $mg/cc \times 10^3$	Uptake mg/cc alumina	$D_{p_2} \times 10^6$ cm^2/sec
+35-65	10.5	16.95	2.36
+24-35	9.8	18.03	2.15

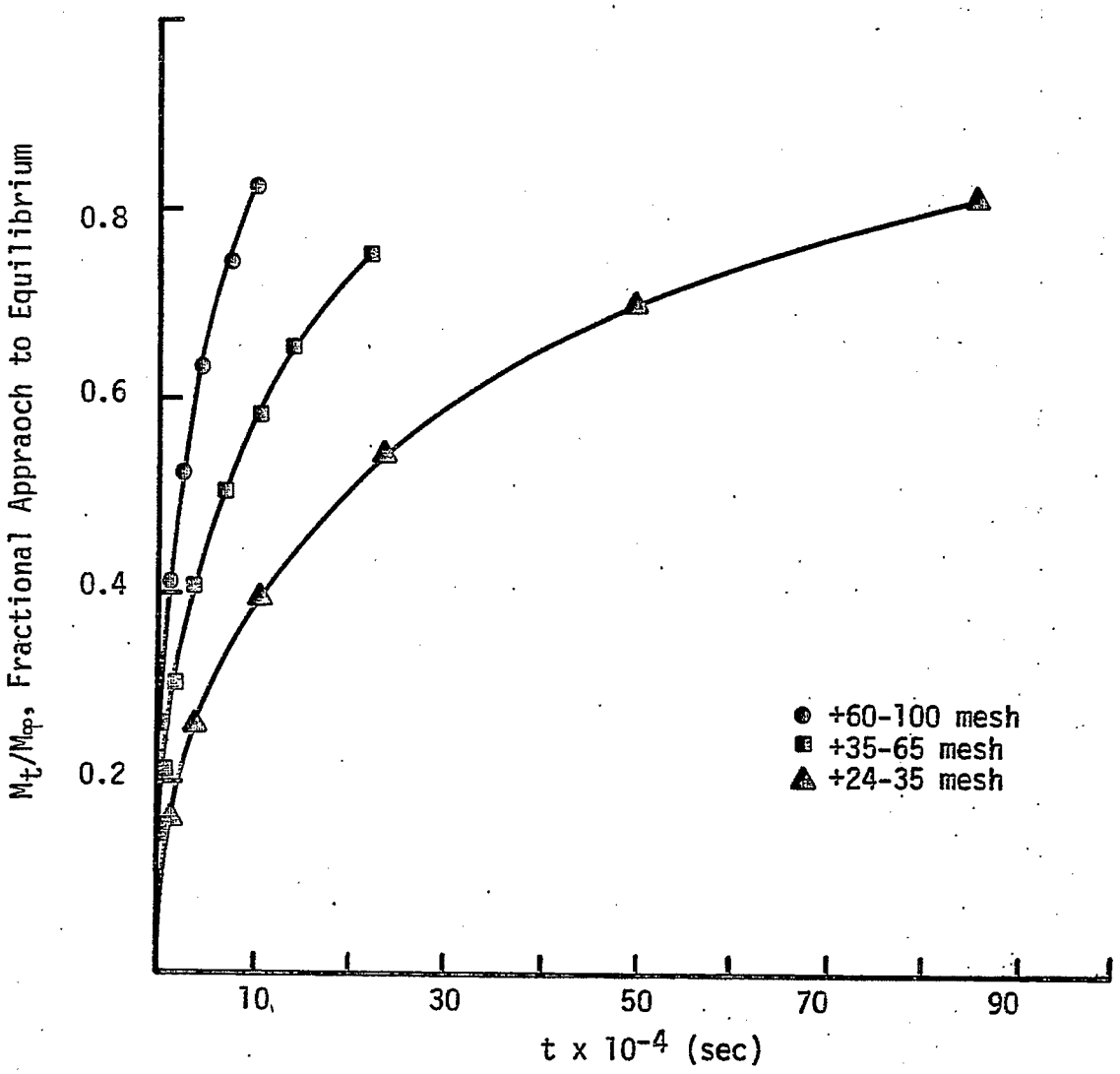

Figure 1. Comparison of the uptake rate for three particle sizes.

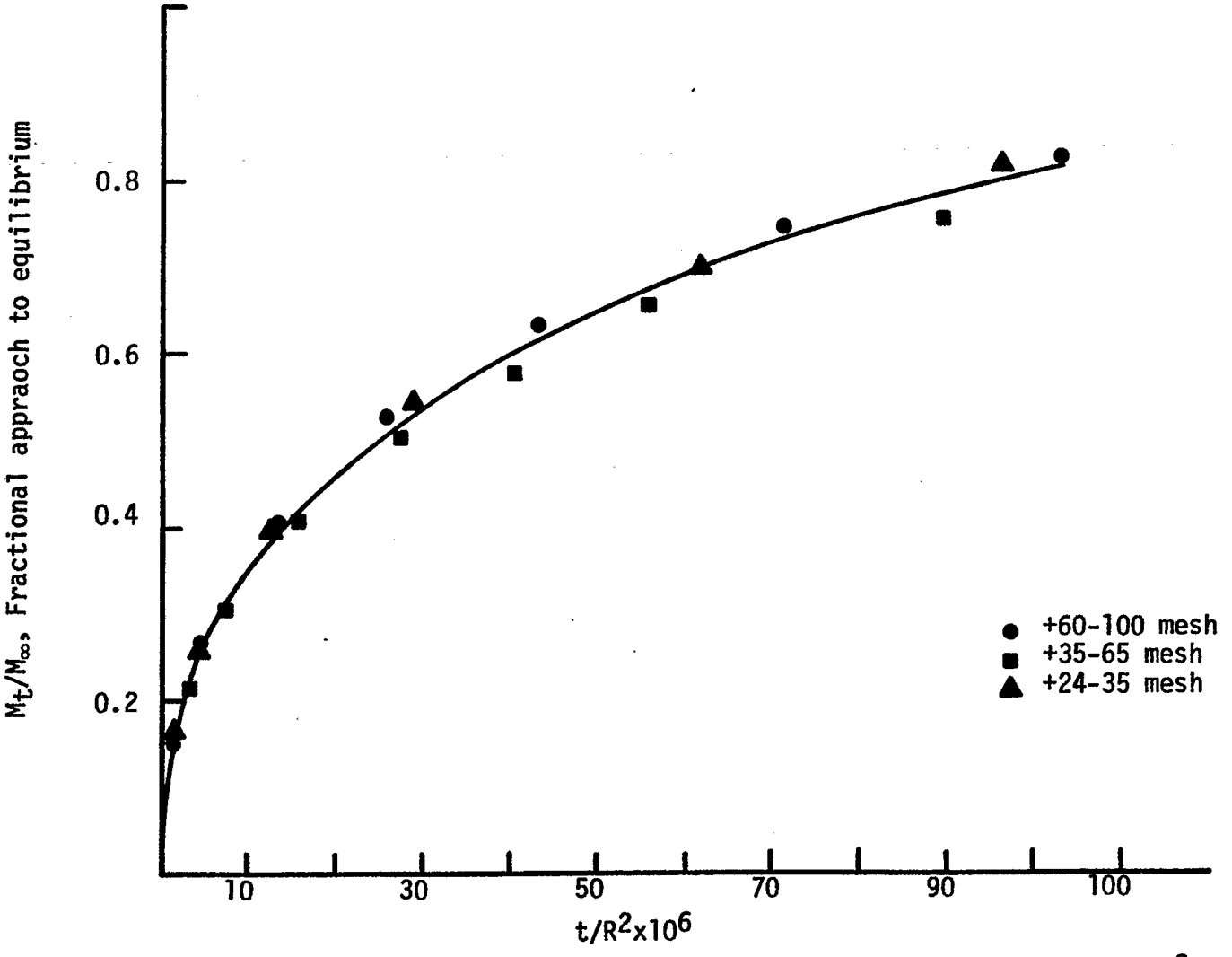

Figure 2. Plot of the uptake of the three particle sizes with t/R^2.

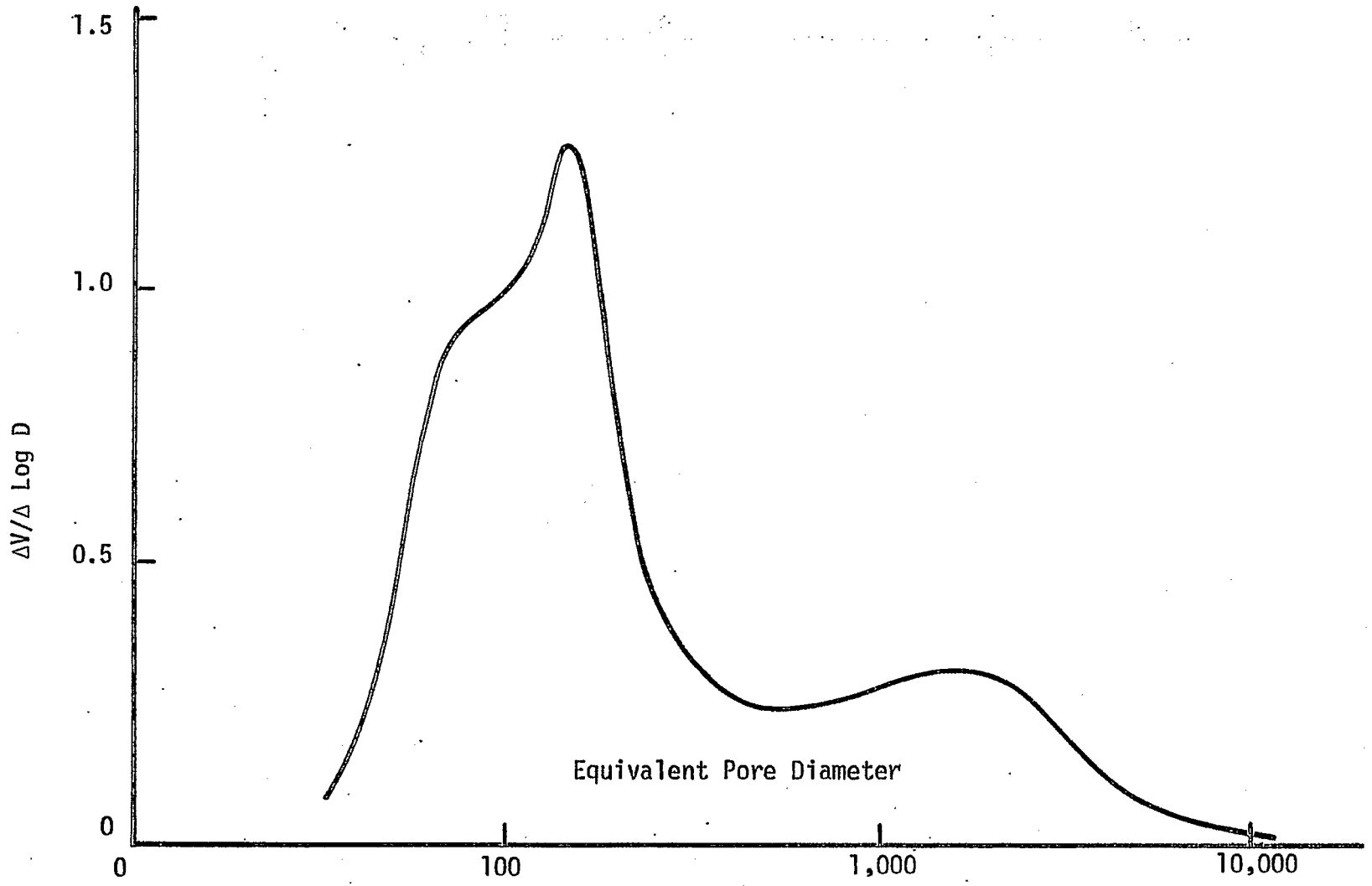

Figure 3. Pore size distribution of bimodal alumina.

Task 13

Catalyst Research and Development

Faculty Advisor: F.V. Hanson
Graduate Student: C.S. Kim

Introduction

The objectives of this project are to develop a preparation technique for a Raney type catalyst (particularly Raney iron-manganese catalyst) and to determine the optimum process variables for the maximum production of gasoline boiling range hydrocarbons, low molecular weight olefins and BTX via the hydrogenation of carbon monoxide. A detailed discussion of the objectives were presented in a previous report.[1]

An electrical heating furnace was built to prepare Al-Fe and Al-Fe-Mn alloys. Several samples of alloys were prepared and the optimum preparation conditions were determined. A stirred tank reactor was fabricated to activate the alloys in an aqueous solution of sodium hydroxide at different activation conditions. A fixed-bed reactor system was built in which catalyst screening tests are being carried out to determine the catalyst composition and activation variables which will optimize the catalyst activity and selectivity. The same reactor system will be used for the process variable investigation.

Project Status

An Al-Fe alloy (Al 53, Fe 47 wt %) was prepared using the same procedures as reported before with one exception. The melted alloy was cooled slowly in the furnace (100°C/hr cooling from 1250°C to 600°C) instead of quickly quenching it on a steel plate. Since the Al-Fe alloys with Al content between 50 to 60 wt % are very brittle and are easily crumbled within a few days of storage, it was speculated that the poor mechanical strength of materials may arise from thermal stresses during rapid quenching. However, the alloy prepared with a slow cooling step was also brittle, as already reported by early workers.[2]

A modified casting method was then used to prepare the Al-Fe alloys. Instead of quenching on a steel plate, the hot melt of alloy was cast into a graphite mold. The product from this casting was less porous and was not as extensively oxidized as the alloy produced by the previous casting method. The alloy cast in the mold was also quite brittle, but it showed less of a tendency to crumble during storage than the one cast on a plate.

An Al-Fe alloy (Al 50, Fe 50 wt %) was prepared by casting in a cylindrical graphite mold with an ID of 1 inch and a height of 5 inches. The above alloy consisted of 76% $FeAl_2$ phase and 24% Fe_2Al_5 phase according to the phase diagram. This alloy was prepared to compare the effect of alloy phase composition on the catalytic activity of Raney iron catalysts with the one prepared from the Fe_2Al_5 phase only. Figure 1 shows a two dimensional

surface picture of the alloy after polishing and etching with 20% sulfuric acid. A positive confirmation of the two phases by microprobe analysis has not yet been successful.

The fixed-bed reactor system underwent preliminary testing to demonstrate its suitability as a catalyst testing unit with samples of the catalysts. A blank run (with no catalyst in the catalyst bed) was made to assess the catalytic activity of the fixed-bed reactor system (the stainless steel tubing and packing materials, i.e., ceramic chips). After reducing the reactor system at 500°C with flowing H_2 for 16 hours, only a trace amount of methane was found from the reaction of CO and H_2 gas (H_2/CO=2) at 235°C and 250°C, respectively.

An Fe-Mn coprecipitated catalyst (Mn/Fe=4.4/100 atomic %) was tested in the fixed-bed reactor to compare it with the results obtained by previous workers in this laboratory. Table 1 shows the results, which do not agree, especially the last three runs at 220, 230 and 240°C. The three runs were made after exposing the catalyst to a CO and H_2 gas mixture for two days due to the failure of the reactor operation. When the catalyst was exposed to the gas mixture and the reaction temperature of 200°C was reduced to room temperature and then reheated, the catalyst surface was activated to a greater extent by carburization. The last three runs show a high level of CO conversion. A strict comparison between the two runs could not be made with only two sets of data, 200 and 210°C. A further comparison study was not attempted due to the unavailability of catalyst samples used by previous workers.

The fixed-bed reactor was modified by installing a gas mass flowmeter (Union Carbide model) in place of a high pressure rotameter to better control in the input reactant gas flow and to improve the input and output mass balance. A far better carbon mass balance based on input and output was possible with the mass flowmeter. Generally, the mass balance was better than $\pm$5% error.

Two types of Raney iron catalysts were tested in the reactor. Catalyst RF-1 was activated with a NaOH solution at 25°C and catalyst RF-2 at 50°C. More detailed information on the conditions of the catalyst activation is listed in the previous report. These catalysts were stored under absolute ethanol at 0°C. After transferring an appropriate amount of catalyst into a sample bottle (with a vacuum valve on top) from the reservoir bottle, the excess ethanol was evacuated by a vacuum pump for about one hour until the sample was completely dry. After weighing the catalyst sample, deionized water was added to the sample bottle through the vacuum valve to immerse the catalyst in water. The water-catalyst slurry was transferred into the reactor. This loading procedure eliminates the exposure of the catalyst to the air. After drying the wet catalyst in the reactor with a stream of H_2 at room temperature for about 5 hours, the CO hydrogenation reaction was initiated after heating the reactor to the desired reaction temperature (about 200°C range) and introducing the gas mixture. During the heating period (about 1 hour) the catalyst must have been reduced to some extent under H_2 gas stream.

Exploratory tests were made with two Raney iron catalysts to find an optimum range of the reaction variables such as temperature and space

velocity, which will give low levels of CO conversion which insure nearly isothermal reaction conditions. Table 2 shows the results from the runs with the RF-1 catalyst and compares them with the results from the runs with the precipitated iron catalyst.[3] The catalytic activity of the RF-1 catalyst for CO hydrogenation is higher than that of the precipitated one. This is based on the CO conversion level with the former catalyst being tested at a space velocity at nearly two times that of the precipitated one. The general trend of the data upon increasing the reaction temperature is in agreement with the one observed by the previous workers. As the temperature increases, the methane content in the product decreases while the C_2-C_4 and C_5^+ fraction content increases. The O/P ratio is somewhat lower with catalyst RF-1 than that of the precipitated iron catalyst.

The data with superscript b are obtained from the initial stage of the reaction, i.e., within a few hours of the start of the run. The high conversion level (extremely rare) at 200°C and 210°C indicates a high initial catalytic activity, probably induced by the chemisorbed H_2 on the surface of the RF-1. The high content of chemisorbed H_2 on the RF-1 surface explains the high methane product yield and low O/P ratio due to the dominant hydrogenation, which leads to increased paraffin formation. A more detailed study has to be done on the variation of catalytic activity with reaction time to provide a meaningful catalyst screening test.

Table 3 shows some results obtained from the RF-2 catalyst. The catalytic activity of RF-2 catalyst is similar to that of the precipitated one, while the selectivity for olefins is somewhat lower above 210°C. The trend of the product distribution with an increase in temperature is the same as in the RF-1 case. The catalytic activity of the RF-1 for CO hydrogenation is higher than that of the RF-2 catalyst as seen in Tables 2 and 3. The higher activity of the RF-1 may be due to the relative abundance of α-Fe in a catalyst activated at low temperature while the one activated at higher temperatures contains more iron oxides as reported by Schwartzendruber.[4] However, further study is needed to explain the differences in activity.

The total surface area of the RF-1 and RF-2 catalysts were determined by nitrogen adsorption using a Micrometrics Surface Analyzer (Model 2100 D). The RF-1 and RF-2 has a 40 m^2/g and 49 m^2/g surface area, respectively.

Future Work

A detailed study of the in-situ catalyst activation process (TGA reduction study) will be carried out. The chemisorptive capacity of the reduced, activated Raney catalysts will be determined to assess the efficacy of the reduction procedure (determined from TGA study). The selectivity and activity of the reduced catalysts will be determined at a standard set of operating variables so that the optimum catalyst composition and activation variables can be specified for use in the process variable study.

References

1. W.H. Wiser et al., DOE Contract No. DE-AC01-79 ET14700-6, Quarterly Progress Report, Salt Lake City, Utah, Jan - Mar 1981.

2. A.G.C. Gwyer and H.W.L. Phillips, J. Inst. Metals, 38, 35 (1927).

3. Y. Tsai, M.S. Thesis, University of Utah, Salt Lake City, Utah, 1980.

4. L.J. Schwartzendruber and B.J. Evans, J. Catal., 43, 207 (1976).

Table 1. CO hydrogenation with coprecipitated catalyst.

Reaction Temp (°C)	CO Conversion	Hydrocarbon Selectivity % C_1	C_2-C_4	C_5^+	ROH	O/P
200	3.7 (2.3)	22.2 (30.1)	63.5 (44.9)	11.4 (10.5)	2.9 (14.5)	3.0 (1.3)
210	12.1 (4.0)	19.3 (21.0)	64.6 (39.3)	12.0 (20.2)	4.0 (19.4)	3.1 (1.4)
220	22.5 (5.8)	26.9 (17.3)	60.3 (52.4)	10.8 (16.3)	2.1 (14.0)	2.0 (1.8)
230	30.5 (8.5)	30.2 (12.0)	56.5 (47.4)	10.2 (15.7)	3.1 (24.9)	1.2 (3.0)
240	42.0 (14.1)	36.0 (10.1)	54.5 (48.1)	8.0 (20.5)	1.4 (21.2)	1.8 (3.7)

Reaction conditions: pressure, 500 psig; H_2/CO, 2; space velocity, 1.06 cc/g-cat sec

Data in parentheses are from previous workers.

ROH = total % content of alcohol in hydrocarbon product.

O/P = olefin/paraffin ratio in C_2-C_4 fraction.

Table 2. CO hydrogenation over RF-1 catalyst.

Reaction Temp (°C)	CO% Conversion	Hydrocarbon Selectivity % C_1	C_2-C_4	C_5^+	O/P
180	1.6	44.2	46.0	9.9	0.94
190	3.4	39.3	49.7	11.0	0.68
200	6.1	36.0	50.9	13.1	0.60
200[a]	(3.2)	(33.5)	(53.7)	(11.9)	(1.12)
200[b]	(96.4)	(82.4)	(17.2)	(0.4)	(0.0)
210	10.0	33.8	52.2	14.0	0.60
210[a]	(4.2)	(23.8)	(52.5)	(18.8)	(1.09)
210[b]	(98.2)	(77.5)	(21.6)	(0.9)	(0.006)

Reaction Conditions: pressure, 500 psig; H_2/CO, 2; space velocity, 2.39 cc/g-cat sec.
[a]Data obtained with a precipitated Fe catalyst at a space velocity of 1.06 cc/g-cat sec.
[b]Data from the initial stage of reaction time.

Table 3. CO hydrogenation over RF-2 catalyst.

Reaction Temp (°C)	CO% Conversion	C_1	C_2-C_4	C_5^+	O/P
190	1.8	45.8	43.0	10.9	1.0
200	4.2 (3.2)	35 (33.5)	40.5 (53.7)	13.8 (11.9)	1.0 (1.1)
210	7.2 (4.2)	36.3 (28.8)	45.9 (52.5)	16.6 (16.9)	0.78 (1.2)
220	11.5 (10.2)	35.0 (23.8)	45.9 (52.5)	17.5 (18.8)	0.62 (1.09)
230	16.8	35.0	47.0	14.6	0.50

Reaction Conditions: pressure, 500 psig; H_2/CO, 2; space velocity, 1.06 cc/g-cat sec.
Data in parentheses are from precipitated iron catalyst.

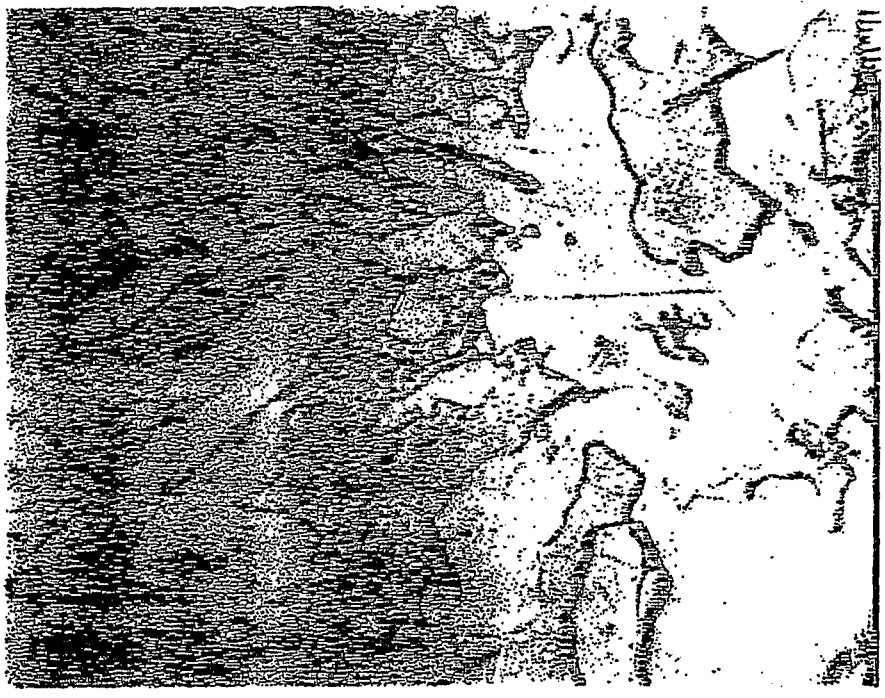

Figure 1. An optical micrograph of an Al-Fe (50:50 wt %) alloy. 500 X, sample etched with 20% sulfuric acid at 70°C for 30 sec.

Task 13

Catalyst Research and Development

Synthesis of Light Hydrocarbons from CO and H_2

Faculty Advisor: F.V. Hanson
Graduate Student: Y.S. Tsai

Introduction

The production of low molecular weight olefins (C_2-C_4) from the hydrogenation of carbon monoxide has been investigated over unsupported iron-manganese catalysts. The results from the preliminary tests which were performed in a bench-scale fixed-bed reactor system showed that the unsupported iron-manganese catalyst was very selective in the production of C_2-C_4 olefins. Data on the screening tests of sixteen iron-manganese catalysts indicated that a catalyst composed of 2 parts of manganese per 100 parts of iron was the most selective of iron-manganese catalysts. The effects of the process variables were also studied. The results mostly agreed with those found in the literature.

The new fixed-bed reactor system designed to obtain a more accurate analysis of the products has been under fabrication and is close to completion. The calculation of the material balance for the synthesis in this new system will be more comprehensive due to the accuracy of the analyses for the inputs and the outputs. The other objectives of this project include a better understanding of the catalyst nature corresponding to its activity and selectivity, the procedure of the catalyst pretreatment for the maximum production of C_2-C_4 olefins and the study of a comprehensive process variable effects.

Project Status

The flow diagram of the new fixed-bed reactor system was shown in the previous report. Two installation changes have been made. The metering valve was relocated in front of the rotameter and a shut-off valve was installed where the metering valve had been. The fabrication of the system is close to completion. All the equipment has been performance tested. Since poisonous gases will be used, tests will be undertaken to check for leaks.

Future Work

Iron-manganese catalysts will be prepared by the coprecipitation method. Tests on the catalyst activity will be performed. The characterization of the catalyst will be initiated to understand the catalyst nature corresponding to its activity and selectivity. The literature survey on the synthesis of light hydrocarbons via the carbon monoxide hydrogenation will be continued.

Task 14

Characterization of Catalysts and Mechanistic Studies

Faculty Advisor: F.E. Massoth
Graduate Student: K.B. Jensen

Introduction

This phase of the project is intended to supplement the high pressure reactor studies by detailed examination of the catalyst properties which enhance catalyst activity and selectivity. This is accomplished by characterization studies performed on fresh catalysts and on the same catalysts which have been run in the reactor. Of particular interest are metal areas, phase structure, catalyst stability and surface characteristics. Also, variables in catalyst preparation and pretreatment are examined to establish their effects on catalyst properties. Finally, in-situ adsorption and activity are studied under modified reaction conditions with a number of well-characterized catalysts to obtain correlating relationships. The catalysts under present investigation are iron-based catalysts promoted with manganese oxide.

Previous work had shown the reduced catalysts have low surface areas (<10 m^2/g) and are composed of two principal phases, α iron and manganese (II) oxide. Some used catalysts were also found to contain small amounts of possible iron oxide and iron carbide phases. Investigations using the scanning electron microscope indicated that the MnO phase is well dispersed in the catalysts and X-ray line broadening results indicated that the MnO particles or possible layers average in the order of 200 Å in breadth. Some iron (II) oxide (FeO) is also indicated to be present in the MnO phase by X-ray diffraction.

Preliminary carburization studies gave two general regimes of carburization, an early fast carburization followed by a slower one. The presence of MnO promoter was found to slow carburization.

Temperature programmed reaction/desorption studies support the interpretation of some dissociative chemisorption of CO on the iron containing catalysts; also that a relatively strong interaction exists between the catalysts and both adsorbed carbon and oxygen. The pure MnO catalyst was found to be generally inactive toward CO but did adsorb CO_2 and O_2.

Data from X-ray diffraction, BET surface area, and CO and O_2 chemisorption experiments have been used to produce tentative structural models for the low manganese and high manganese iron catalysts. The low manganese catalysts have a significant portion of their potential iron surface area covered by smaller particles of manganese oxide. The high manganese catalysts seem to be iron and MnO particles showing relatively little interaction.

Initial transmission electron microscopy (TEM) studies have shown the catalysts to be assemblages of spheroidal particles with the basic particle ranging in size from roughly 500 Å to 5000 Å. These particles were usually found in clumps. The low manganese-iron catalysts had particle surfaces that contained globular and often filament like protuberances. These surface structures presumably are composed mainly of MnO promoter but no direct identification was possible using TEM.

Project Status

Carbon monoxide conversion over several iron-manganese catalysts was measured using a 5% CO in H_2 reactant gas. Conversion was measured at three temperatures using a flow microreactor and an on-line gas chromatograph. Rate constants were determined assuming a pseudo first order rate expression. Results for the freshly reduced catalysts are shown in Table 1. Generally, the activity on a weight basis decreased substantially with the addition of a small amount of manganese promoter and then decreased gradually with increasing manganese content. This trend mirrors preliminary data on iron surface areas of the catalysts. Specific catalyst activities are not given because some iron areas are still being confirmed.

The catalysts were also carburized 3 hr at 250°C in $H_2/CO = 2.0$ synthesis gas and the CO hydrogenation activity was again measured at the same conditions as previously reported. The basic performance of the catalysts was very similar to the freshly reduced catalysts, although overall activities decreased slightly from the initial values (Table 2). It is interesting to note that carburizing the catalysts did not profoundly affect the CO hydrogenation activity as it did the hexene hydrogenation activity reported previously.[1] The measured activation energies were slightly below those found in the high pressure reactor studies.[2]

Several catalyst samples were also examined by ESCA using a Hewlett Packard Electron Spectrometer. The catalysts had been prereduced in H_2 at 500°C and passivated by slowly exposing to air at room temperature. Samples were finely powdered and placed on double stick tape before introduction into the spectrometer. Because of the surface sensitivity of ESCA analysis, this technique provides a very good method of semi-quantitatively measuring the Mn/Fe ratio present on the surface of the catalysts. The results are shown in Table 3. Two portions of the ESCA spectra containing Mn and Fe peaks are compared. The $2P_{3/2}$ peaks of Mn and Fe are core electron peaks and are somewhat more surface sensitive than the 3S peaks. The peak areas are adjusted by a cross section "sensitivity factor" (∇) for the element peak in question.

In all cases, the presence of manganese promoter resulted in a higher Mn surface concentration than the bulk molar composition. Carburization was found to have little effect upon the Mn/Fe peak ratio. These results are in agreement with selective chemisorption data showing that manganese concentrates on the surface of the iron particles, covering part of the iron surface. The manganese promoter coverage is more than a few monolayers deep as evidenced by the overall similarity of the ratios derived from the $2P_{3/2}$ and 3S peaks.

Future Work

Additional TEM studies are still pending and work is continuing on selective chemisorption.

References

1. W.H. Wiser, F.E. Massoth and K.B. Jensen, DOE Contract No. De-AC01-79ET14700, Quarterly Progress Report, Salt Lake City, Utah, Jan-Mar 1981.

2. Y. Tsai, M.S. Thesis, University of Utah, Salt Lake City, Utah, 1980.

Table 1. Freshly Reduced Fe-Mn Catalyst Activity.

	k_{CO}[b] (cc/min g cat)			
Cat.[a]	200°C	250°C	300°C	Ea[c] (Kcal/mole)
C-0	7.4	34.0	(high)	15
C-3	2.1	8.2	28.3	14
C-29	1.7	8.6	31.0	16
C-52	0.9	6.5	14.2	15
C-74	1.4	3.8	10.1	11

[a]Numbers refers to mole percent Mn.

[b]First order rate constant for CO conversion.

[c]Activation energy.

Table 2. Carburized Fe-Mn Catalyst Activity.[a]

	k_{CO}			
Cat.	200°C	250°C	300°C	Ea (Kcal/mole)
C-0	7.5	32.0	55	11
C-3	1.6	6.9	27.6	15
C-29	0.9	7.5	25.1	18
C-52	1.9	2.6	10.1	9
C-74	1.3	4.4	7.9	10

[a]Catalysts were carburized 3 hr in $H_2/CO = 2.0$ synthesis gas at 250°C prior to testing.

Table 3. ESCA Peak Area Ratios.

Catalyst	Bulk Mole Ratio Mn/Fe	$\frac{Mn\text{-}2P_{3/2}/\nabla Mn}{Fe\text{-}2P_{3/2}/\nabla Fe}$	$\frac{Mn\text{-}3S/\nabla Mn}{Fe\text{-}3S/\nabla Fe}$
C-0	0	0	0
C-5	0.056	2.25	1.12
C-5[a]	0.056	1.71	0.78
C-39	0.631	8.79	11.8
C-74	2.77	14.7	-
Phys. Mix[b]	0.786	0.86	0.42

[a]Carburized 3 hr at 250°C in $H_2/CO = 2.0$.

[b]Mixture of C-0 (pure Fe) and C-100 (pure MnO).

V. Conclusions

Detailed conclusions are included in the reports for each task. Task 4 is no longer funded and has been discontinued. No report was submitted for Task 2. No work was done under Task 15.

☆U.S. GOVERNMENT PRINTING OFFICE: 1981-740-145 2767